

Inexact Newton combined approximations in the topology optimization of geometrically nonlinear elastic structures and compliant mechanisms

T. A. Senne¹, F. A. M. Gomes², and S. A. Santos²

¹ *Institute of Science and Technology, Federal University of São Paulo, Avenida Cesare Mansueto Giulio Lattes, 1201, 12247-014, São José dos Campos, Brazil. Email: senne@unifesp.br*

² *Institute of Mathematics, University of Campinas, Rua Sergio Buarque de Holanda, 651, 13083-859, Campinas, São Paulo, Brazil*

Emails: [sasantos@unicamp.br](mailto:santos@unicamp.br), chico2@unicamp.br

December 17, 2021

Abstract

This work blends the inexact Newton method with iterative combined approximations (ICA) for solving topology optimization problems under the assumption of geometric nonlinearity. The density-based problem formulation is solved using a sequential piecewise linear programming (SPLP) algorithm. Five distinct strategies have been proposed to control the frequency of the factorizations of the Jacobian matrices of the nonlinear equilibrium equations. Aiming at speeding up the overall iterative scheme while keeping the accuracy of the approximate solutions, three of the strategies also use an ICA scheme for the adjoint linear system associated with the sensitivity analysis. The robustness of the proposed reanalysis strategies is corroborated by means of numerical experiments with four benchmark problems – two structures and two compliant mechanisms. Besides assessing the performance of the strategies considering a fixed budget of iterations, the impact of a theoretically supported stopping criterion for the SPLP algorithm was analyzed as well.

Keywords: topology optimization; geometric nonlinearity; approximate reanalysis; combined approximations; inexact Newton

MSC (2020): 90C30; 65K05; 47J25; 65J15; 74B20

1 Introduction

One of the most common problems in topology optimization is the minimization of the mean compliance of structures, under the constraints of static equilibrium and a prescribed volume of material [7]. In several circumstances, the requirements upon the structure may impose an elastic but nonlinear relation between strains and displacements, meaning that the structure is under geometric nonlinearity. In such a case, the computation of the objective function of the topology optimization problem demands the solution of a system of nonlinear equations that models the nodal displacements of the structure due to the external forces. When it comes to compliant mechanisms, under the geometric nonlinearity assumption, addressing nonlinear systems of equations is mandatory as well. The approximate solutions of these systems are usually computed by Newton's method, constituting, by far, the most expensive step in the process of achieving optimal configurations.

Several attempts have been made to reduce the effort spent to compute the nodal displacements of the structures and mechanisms [21]. Challenges such as parallel and numerical scalability have been pursued, specially when it comes to 3-D problems (see e.g. [1] and references therein). The

use of preconditioned conjugate gradients has been exploited in the solution of the linear systems associated with the equilibrium equations [4, 5, 23, 24]. Meshless-based local reanalysis [12] and a meshfree reduced basis approach for large deformations [26] have been analyzed as well. In the last years, educational codes handling geometric nonlinearity, based on the SIMP (Solid Isotropic Material with Penalization) method [10, 29], and on the BESO (Bi-directional Evolutionary Structural Optimization) method [17], also became available. The recent survey [25] discusses additional aspects concerning high-performance computing, approximate reanalysis, reduced-order modeling, and multigrid methods.

Inspired on the *combined approximations* approach [3, 8, 20], we have analyzed some strategies that merge the inexact Newton scheme with iterative combined approximations for minimizing the mean compliance of structures and for maximizing the displacement of compliant mechanisms. Our approach rests upon a sequential piecewise linear programming (SPLP) algorithm [16] that, aside from having a stopping criterion with theoretical support, has proven to be efficient and robust. In a previous work [28], the approximate reanalysis technique has been applied in combination with the SPLP algorithm to solve three benchmark structure problems under small displacements. In the current work, besides addressing two structures, we have also applied the devised strategies to the design of two mechanisms. A detailed analysis of the results has been reported, assessing the scope and the impact of the methodology.

This text is organized as follows. The problem formulation is presented in Section 2. The elements of the reanalysis technique that encompasses the inexact Newton method with iterative combined approximations are detailed in Section 3. The experimental setup is provided in Section 4, namely the test problems, the proposed strategies and the implementation details. The analysis of the performance of the strategies with a fixed budget is done in Section 5, whereas Section 6 presents the results concerning the effect of the mesh refinement. The convergence performance of the SPLP with the nonlinear reanalysis is reported in Section 7. The behavior of $\|\mathbf{B}\|_2$ is assessed in Section 8, and Section 9 contains our final remarks.

2 Problem formulation

Suppose that Ω is the design domain of a structure. In the context of topology optimization, we want the distribution of material on the domain Ω to be optimal in some sense, satisfying certain constraints. In this work, we consider that Ω is two-dimensional and, with the aim of making the problem computationally affordable, we discretize it into rectangular finite elements, using bilinear interpolating functions to approximately evaluate the displacements.

Let Ω_d be the discretized domain, partitioned in disjointed subdomains Ω_i , i.e. $\Omega_d = \cup_{i=1}^{n_{el}} \Omega_i$. We denote by n_{el} the number of elements of Ω_d and by n_{nd} the number of its nodes. We associate with each Ω_i a continuous variable ρ_i representing the density of material, in such a way that $\rho_i = 1$ if the element is solid or $\rho_i = 0$ if the element is void.

We address two topology optimization problems: the compliance minimization of rigid structures and the displacement maximization of compliant mechanisms. In both cases, the optimization problem can be stated as

$$\begin{aligned} \min_{\boldsymbol{\rho}} \quad & \mathbf{l}^T \mathbf{u} \\ \text{s.t.} \quad & \mathbf{r}(\mathbf{u}, \boldsymbol{\rho}) = \mathbf{0} \\ & \sum_{i=1}^{n_{el}} v_i \rho_i = V^* \\ & 0 < \rho_{\min} \leq \rho_i \leq 1, \quad i = 1, \dots, n_{el}, \end{aligned} \tag{1}$$

where $\boldsymbol{\rho} \in \mathbb{R}^{n_{el}}$ is the vector of densities of each element of Ω_d (that are our design variables), $\mathbf{u} \in \mathbb{R}^{2n_{nd}}$ is the vector of nodal displacements, v_i is the volume of the i -th element, V^* is the prescribed volume of the structure, and ρ_{\min} is a sufficiently small positive number used to avoid numerical instabilities. For the compliance minimization of rigid structures, $\mathbf{l} \in \mathbb{R}^{2n_{nd}}$ is the

vector of nodal external forces, \mathbf{f} , and in the case of the maximization of the displacements for compliant mechanisms it is a vector filled with zeros, except at the positions corresponding to the output points (the points in which the displacement is to be maximized), where it is equal to -1 . We remark that, since we adopt the SIMP interpolation model [6], \mathbf{u} depends on the vector of densities $\boldsymbol{\rho}$, so we can express $\mathbf{u} \equiv \mathbf{u}(\boldsymbol{\rho})$.

The system

$$\mathbf{r}(\mathbf{u}, \boldsymbol{\rho}) = \mathbf{0} \quad (2)$$

represents the static equilibrium conditions of the structure (or compliant mechanism). Under the assumption of geometric nonlinearity, we have

$$\mathbf{r}(\mathbf{u}, \boldsymbol{\rho}) = \mathbf{f}_{int}(\mathbf{u}, \boldsymbol{\rho}) - \mathbf{f}, \quad (3)$$

where $\mathbf{f}_{int}(\mathbf{u}, \boldsymbol{\rho}) \in \mathbb{R}^{2n_{nd}}$ is the vector of internal nodal forces. We say that $\mathbf{r}(\mathbf{u}, \boldsymbol{\rho})$ in (3) is the *residual* associated with the nonlinear system (2).

Usually, the Newton-Raphson method (that, from now on, will be referred as *Newton's method*) is used to find an approximate solution for the nonlinear system (2). Given an initial point $\mathbf{u}^{(0)}$ and keeping $\boldsymbol{\rho}$ fixed, at each iteration of Newton's method, we solve the linear system

$$\mathbf{K}_T(\mathbf{u}^{(\ell)}, \boldsymbol{\rho})\mathbf{s} = -\mathbf{r}(\mathbf{u}^{(\ell)}, \boldsymbol{\rho}), \quad (4)$$

where $\mathbf{K}_T \equiv \mathbf{K}_T(\mathbf{u}, \boldsymbol{\rho}) \in \mathbb{R}^{2n_{nd} \times 2n_{nd}}$ is the Jacobian matrix of the nonlinear system (2), also known as the *global tangent stiffness matrix*, that is supposed to be nonsingular. The solution of the linear system (4), denoted by $\mathbf{s}^{(\ell)}$, is used to obtain the new approximate solution, $\mathbf{u}^{(\ell+1)} = \mathbf{u}^{(\ell)} + \mathbf{s}^{(\ell)}$. Usually, we consider that $\mathbf{u}^{(\ell)}$ is a good approximate solution to the original nonlinear system (2) whenever $\|\mathbf{r}(\mathbf{u}^{(\ell)}, \boldsymbol{\rho})\| < \varepsilon$, where ε is a prescribed small positive number.

It is important to mention that the definitions of the global tangent stiffness matrix \mathbf{K}_T and of the residual \mathbf{r} depend on the hyperelastic model for the material of the structure. In this work, we adopt the neo-Hookean material model of Simo-Ciarlet [22], combined with the SIMP model, so we have

$$\mathbf{K}_T(\mathbf{u}, \boldsymbol{\rho}) = \sum_{i=1}^{n_{el}} \rho_i^p \int_{\Omega_i} \mathbf{G}^T \mathbf{D}_i \mathbf{G} \, d\Omega_i \quad \text{and} \quad \mathbf{f}_{int}(\mathbf{u}, \boldsymbol{\rho}) = \sum_{i=1}^{n_{el}} \rho_i^p \int_{\Omega_i} \mathbf{G}^T \boldsymbol{\sigma}_i \, d\Omega_i,$$

in which p is the penalty parameter of the SIMP model ($p > 1$), $\mathbf{G} \in \mathbb{R}^{4 \times 8}$ is the matrix of the derivatives of the shape function with respect to the displacements and, for the domain Ω_i of the i -th element of the discretized domain Ω_d , $\mathbf{D}_i \in \mathbb{R}^{4 \times 4}$ is the tangent stiffness modulus matrix and $\boldsymbol{\sigma}_i \in \mathbb{R}^4$ is the first Piola-Kirchhoff stress tensor.

3 Inexact Newton with Iterative Combined Approximations

The factorization of \mathbf{K}_T is the most expensive step in the process of solving the linear system (4). Although the Cholesky factorization is usually employed for symmetric matrices, the LDL^T factorization [15] is required here, since \mathbf{K}_T is not necessarily positive definite. With the aim of saving computational effort, several reanalysis techniques were proposed in the literature. One of the most common reanalysis strategy, named *Combined Approximations* (CA), will be summarized here to ground our presentation, following the lines presented by Amir, Kirsch and Sheinman [3] and by Senne, Gomes and Santos [28].

First of all, let \mathbf{K}_{T0} be the Jacobian at the i -th iteration of Newton's method. Supposing that its factorization is available, it will be reused at the subsequent m iterations $i+1$, $i+2$, \dots , $i+m$, and updated at the iteration $i+m+1$. Denoting by \mathbf{K}_T the Jacobian at the $(i+j)$ -th iteration (with $1 \leq j \leq m$), we can rewrite the linear system (4) as

$$(\mathbf{K}_{T0} + \Delta\mathbf{K})\mathbf{s} = -\mathbf{r}, \quad (5)$$

where $\Delta \mathbf{K} := \mathbf{K}_T - \mathbf{K}_{T0}$. After rearranging the terms in (5), we obtain

$$\mathbf{s} = \tilde{\mathbf{s}} - \mathbf{B}\mathbf{s}, \quad (6)$$

where

$$\tilde{\mathbf{s}} := -\mathbf{K}_{T0}^{-1}\mathbf{r} \quad \text{and} \quad \mathbf{B} := \mathbf{K}_{T0}^{-1}\Delta \mathbf{K}. \quad (7)$$

So, using (6), we state the following sequence of steps:

$$\mathbf{s}^{(k+1)} = \tilde{\mathbf{s}} - \mathbf{B}\mathbf{s}^{(k)}, \quad k = 0, 1, 2, \dots \quad (8)$$

Choosing $\mathbf{s}^{(0)} = \tilde{\mathbf{s}}$, the CA strategy consists in generating the first q terms of the sequence (8) to build an approximate solution $\hat{\mathbf{s}}$, given by

$$\hat{\mathbf{s}} = y_1\mathbf{s}^{(1)} + y_2\mathbf{s}^{(2)} + \dots + y_q\mathbf{s}^{(q)} = \mathbf{S}_B\mathbf{y}, \quad (9)$$

where

$$\mathbf{S}_B = [\mathbf{s}^{(1)} \ \mathbf{s}^{(2)} \ \dots \ \mathbf{s}^{(q)}] \quad \text{and} \quad \mathbf{y} = [y_1 \ y_2 \ \dots \ y_q]^T.$$

We remark that q should be a small integer. Usually, $q \leq 10$.

The vector of coefficients \mathbf{y} is found by solving the small ($q \times q$) linear system

$$\mathbf{S}_B^T \mathbf{K}_T \mathbf{S}_B \mathbf{y} = -\mathbf{S}_B^T \mathbf{r},$$

obtained by substituting $\hat{\mathbf{s}}$ in the original linear system (4) and then multiplying both sides of the resulting equation on the left by \mathbf{S}_B^T . Generally, the relative norm of the residual of the linear system (4) is the measure adopted to decide if the approximate solution $\hat{\mathbf{s}}$ will be accepted.

In this work, we propose a new iterative method to get an approximate solution to the linear system (4), named *Iterative Combined Approximations* (ICA), based on the sequence $\{\mathbf{s}^{(k)}\}_{k=0}^{+\infty}$ defined in (8), and described below. It is worth mentioning that a distinct iterative CA approach to address topological modifications for the static reanalysis of structures has been presented in [11].

Given $\tilde{\mathbf{s}}$ as in (7), and any initial point $\mathbf{s}^{(0)}$, the general term of the sequence (8), for any k , can be written as

$$\mathbf{s}^{(k+1)} = [\mathbf{I} - \mathbf{B} + \mathbf{B}^2 - \mathbf{B}^3 + \dots + (-1)^k \mathbf{B}^k] \tilde{\mathbf{s}} + (-1)^{k+1} \mathbf{B}^{k+1} \mathbf{s}^{(0)}. \quad (10)$$

By considering any vector p -norm and the consistent norm of operators, if $\|\mathbf{B}\| < 1$, the matrix $\mathbf{I} + \mathbf{B}$ is nonsingular (cf. [15, §2.3.4]), and its inverse can be expressed by means of the Neumann's series [19, 30, 31]

$$(\mathbf{I} + \mathbf{B})^{-1} = \sum_{j=0}^{+\infty} (-1)^j \mathbf{B}^j.$$

Notice that, from (7), since $\mathbf{B} = \mathbf{K}_{T0}^{-1} \mathbf{K}_T - \mathbf{I}$, as long as \mathbf{K}_T does not differ too much from \mathbf{K}_{T0} , the assumption $\|\mathbf{B}\| < 1$ is reasonable.

Defining $\mathbf{s}^* := (\mathbf{I} + \mathbf{B})^{-1} \tilde{\mathbf{s}}$, from (10) we have

$$\mathbf{s}^{(k+1)} - \mathbf{s}^* = - \left[\sum_{j=k+1}^{+\infty} (-1)^j \mathbf{B}^j \right] \tilde{\mathbf{s}} + (-1)^{k+1} \mathbf{B}^{k+1} \mathbf{s}^{(0)}. \quad (11)$$

Since

$$\begin{aligned} \sum_{j=k+1}^{+\infty} (-1)^j \mathbf{B}^j &= (-1)^{k+1} \mathbf{B}^{k+1} + (-1)^{k+2} \mathbf{B}^{k+2} + (-1)^{k+3} \mathbf{B}^{k+3} + \dots \\ &= (-1)^{k+1} \mathbf{B}^{k+1} (\mathbf{I} - \mathbf{B} + \mathbf{B}^2 - \mathbf{B}^3 + \dots) \\ &= (-1)^{k+1} \mathbf{B}^{k+1} (\mathbf{I} + \mathbf{B})^{-1}, \end{aligned} \quad (12)$$

substituting (12) into (11), we obtain

$$\begin{aligned}\mathbf{s}^{(k+1)} - \mathbf{s}^* &= (-1)^{k+1} \mathbf{B}^{k+1} [\mathbf{s}^{(0)} - (\mathbf{I} + \mathbf{B})^{-1} \tilde{\mathbf{s}}] \\ &= (-1)^{k+1} \mathbf{B}^{k+1} [\mathbf{s}^{(0)} - \mathbf{s}^*]\end{aligned}\tag{13}$$

and hence

$$0 \leq \|\mathbf{s}^{(k+1)} - \mathbf{s}^*\| \leq \|\mathbf{B}\|^{k+1} \|\mathbf{s}^{(0)} - \mathbf{s}^*\|.$$

Once we have $\lim_{k \rightarrow +\infty} \|\mathbf{B}\|^{k+1} = 0$ (provided that $\|\mathbf{B}\| < 1$), and assuming that $\|\mathbf{s}^{(0)} - \mathbf{s}^*\|$ remains bounded, by the Squeeze Theorem we conclude that

$$\lim_{k \rightarrow +\infty} \|\mathbf{s}^{(k+1)} - \mathbf{s}^*\| = 0,$$

and, consequently, $\lim_{k \rightarrow +\infty} \mathbf{s}^{(k+1)} = \mathbf{s}^*$.

Now, we will show that \mathbf{s}^* is the (unique) solution of the linear system $\mathbf{K}_T \mathbf{s} = -\mathbf{r}$ if, and only if, \mathbf{s}^* is the (unique) solution of $(\mathbf{I} + \mathbf{B}) \mathbf{s} = \tilde{\mathbf{s}}$. In fact,

$$\begin{aligned}\mathbf{K}_T \mathbf{s}^* = -\mathbf{r} &\iff (\mathbf{K}_{T0} + \Delta \mathbf{K}) \mathbf{s}^* = -\mathbf{r} \\ &\iff \mathbf{s}^* = -\mathbf{K}_{T0}^{-1} \mathbf{r} - \mathbf{K}_{T0}^{-1} (\Delta \mathbf{K}) \mathbf{s}^* \\ &\iff \mathbf{s}^* = \tilde{\mathbf{s}} - \mathbf{B} \mathbf{s}^* \\ &\iff (\mathbf{I} + \mathbf{B}) \mathbf{s}^* = \tilde{\mathbf{s}}.\end{aligned}$$

Using (13), we observe that

$$\begin{aligned}\mathbf{s}^{(k+1)} - \mathbf{s}^* &= (-1)^{k+1} \mathbf{B}^{k+1} [\mathbf{s}^{(0)} - (\mathbf{I} + \mathbf{B})^{-1} \tilde{\mathbf{s}}] \\ &= (-1) \mathbf{B} (-1)^k \mathbf{B}^k [\mathbf{s}^{(0)} - (\mathbf{I} + \mathbf{B})^{-1} \tilde{\mathbf{s}}] = -\mathbf{B} (\mathbf{s}^{(k)} - \mathbf{s}^*)\end{aligned}$$

and, consequently,

$$\|\mathbf{s}^{(k+1)} - \mathbf{s}^*\| \leq \|\mathbf{B}\| \|\mathbf{s}^{(k)} - \mathbf{s}^*\|.\tag{14}$$

Thus, by (14) and under the assumption that $\|\mathbf{B}\| < 1$, we conclude that the sequence $\{\mathbf{s}^{(k)}\}_{k=0}^{+\infty}$ generated by the ICA method has a linear rate of convergence.

Let $\hat{\mathbf{u}}$ be an approximate solution of the nonlinear system (2) found by means of Newton's method, such that $\|\mathbf{r}(\hat{\mathbf{u}}, \boldsymbol{\rho})\| < \varepsilon$. It can be shown that the partial derivatives of the objective function $F(\boldsymbol{\rho}) = \mathbf{l}^T \mathbf{u}(\boldsymbol{\rho})$ are given by $\partial F / \partial \rho_e = \boldsymbol{\lambda}_e^T \partial \mathbf{r} / \partial \rho_e$, where $\boldsymbol{\lambda}$ is the solution of the adjoint linear system

$$\widehat{\mathbf{K}}_T \boldsymbol{\lambda} = -\mathbf{l},\tag{15}$$

$\widehat{\mathbf{K}}_T$ is the global tangent stiffness matrix evaluated at $\hat{\mathbf{u}}$, and $\boldsymbol{\lambda}_e$ encompasses the components of the vector $\boldsymbol{\lambda}$ associated with the e -th element.

In order to avoid the factorization of $\widehat{\mathbf{K}}_T$ (and, thus, to accelerate the solution of our topology optimization problems), the ICA method can also be applied to find an approximate solution of the linear system (15). As done in (8), we define the sequence

$$\boldsymbol{\lambda}^{(k+1)} = \tilde{\boldsymbol{\lambda}} - \widehat{\mathbf{B}} \boldsymbol{\lambda}^{(k)}, \quad k = 0, 1, 2, \dots$$

where $\tilde{\boldsymbol{\lambda}} = -\mathbf{K}_{T0}^{-1} \mathbf{l}$, $\widehat{\mathbf{B}} = \mathbf{K}_{T0}^{-1} \widehat{\Delta \mathbf{K}}$, $\widehat{\Delta \mathbf{K}} = \widehat{\mathbf{K}}_T - \mathbf{K}_{T0}$, and we take $\boldsymbol{\lambda}^{(0)} = \tilde{\boldsymbol{\lambda}}$. Following the same steps shown above, we can prove that, if $\|\widehat{\mathbf{B}}\| < 1$, the sequence $\{\boldsymbol{\lambda}^{(k)}\}_{k=0}^{+\infty}$ converges to the unique solution $\boldsymbol{\lambda}^* = -\widehat{\mathbf{K}}_T^{-1} \mathbf{l}$ of the linear system (15) with a linear rate of convergence.

4 Test problems, proposed strategies and implementation details

In this section we present the computational settings and choices considered in this work.

4.1 Test problems

In our numerical investigation, we have addressed the two structures and the two compliant mechanisms described below.

Cantilever beam. Fig. 1 (left) shows the design domain for this problem. Following the suggestions of [10], we define $L = 120 \text{ mm}$ and suppose that the material used to construct the structure has a Young’s modulus of 3000 N/mm^2 and a Poisson’s ratio of 0.4. The thickness of the structure is equal to 1 mm . An external load of 120 N is applied downwards at the midpoint of the right side. The structure is supported at the left edge, where all of the nodes are fixed. The domain is discretized into 40000 (400×100) finite elements, and the optimal structure must contain 50 % of the domain’s volume.

Slender beam. The design domain of this structure is presented in Fig. 1 (right), in which $L = 400 \text{ mm}$. An external load of 40 N is applied downwards at the center of the domain’s basis, and the structure is supported at the left and at the right edges, where all of the nodes are fixed. The Poisson’s ratio and the Young’s modulus of the material are, respectively, 0.3 and 3000 N/mm^2 . The structure has a thickness of 1 mm . The domain is discretized into 45000 (600×75) finite elements, and the optimal structure must contain 20 % of the domain’s volume.

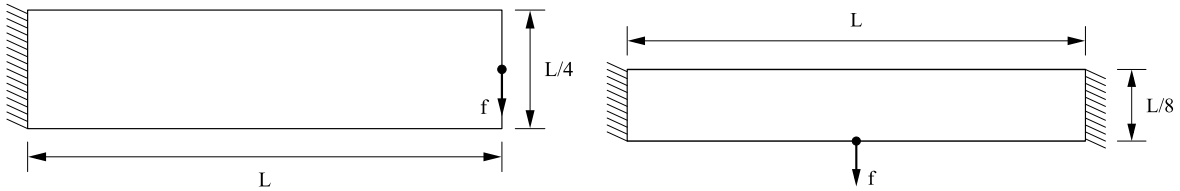


Figure 1: Domains of the structures: cantilever beam (left) and slender beam (right).

Inverter. Fig. 2 (left) exhibits the square domain for the inverter, with $L = 300 \mu\text{m}$ and thickness equal to $7 \mu\text{m}$. At the center of the left edge (point A), there is an external horizontal force of 50 mN pointing to the right. Supports at the lower and the upper left corners prevent horizontal and vertical displacements. The Poisson’s ratio and the Young’s modulus of the material are, respectively, 0.3 and $180 \text{ mN}/\mu\text{m}^2$. The stiffness of the springs of the model at points A (input port) and B (output port) are, respectively, $k_{in} = 4.0 \text{ mN}/\mu\text{m}$ and $k_{out} = 1.0 \text{ mN}/\mu\text{m}$. The volume of the optimal compliant mechanism is limited to 20 % of the domain’s volume. Due to symmetry, only the upper half of the domain is discretized into 45000 (300×150) finite elements.

Gripper. The design domain for the gripper is shown in Fig. 2 (right), where $L = 320 \mu\text{m}$. The domain has a thickness of $7 \mu\text{m}$. In this compliant mechanism, an external force of 4 mN is applied horizontally at point A . Two sets of supports (each one with $L/20 \mu\text{m}$ of length) are located at the upper and lower left corners, preventing displacements. The Poisson’s ratio and the Young’s modulus of the material are, respectively, 0.3 and $180 \text{ mN}/\mu\text{m}^2$. The stiffness of the spring at point A (input port) is $k_{in} = 0.2 \text{ mN}/\mu\text{m}$. At points B and C (output ports), the stiffness is equal to $k_{out} = 1.0 \text{ mN}/\mu\text{m}$. Due to symmetry, only the upper half of the domain is discretized into 51200 (320×160) finite elements. The optimal mechanism must contain 20 % of the domain’s volume.

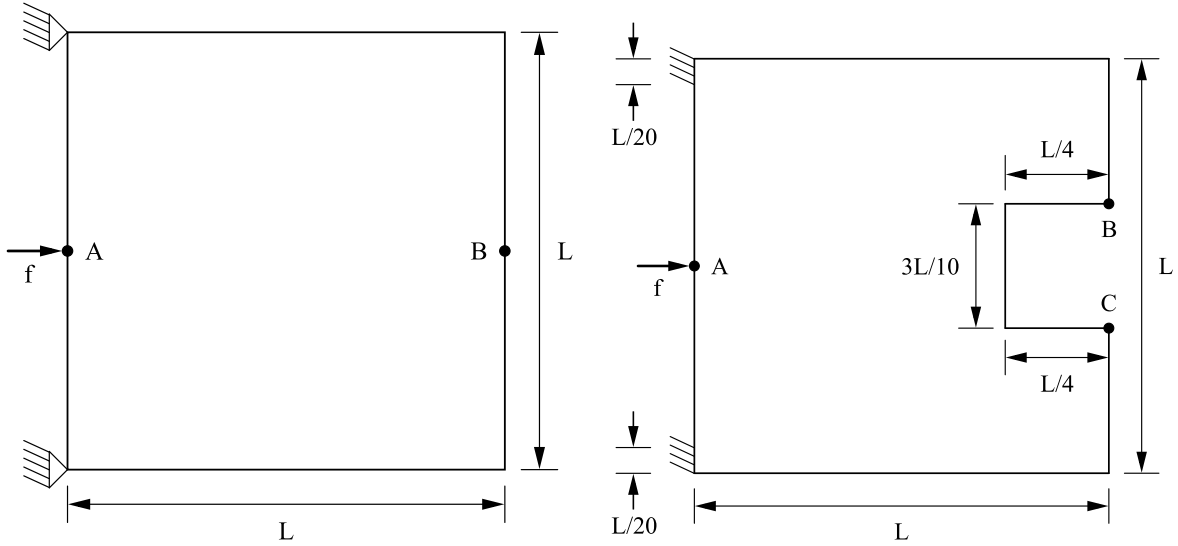


Figure 2: Domains of the mechanisms: inverter (left) and gripper (right).

4.2 Proposed strategies

Whenever the objective function of problem (1) needs to be computed, it is necessary to apply Newton's method to solve the nonlinear system (2), which in turn requires the solution of several linear systems in the form (4). Therefore, the frequency of factorizations of \mathbf{K}_T is the key for speeding up the overall algorithm while keeping the solutions of the system (2) sufficiently accurate.

In the context of the nonlinear analysis of frame structures, Amir, Kirsch and Sheinman [3] presented some strategies based in the pure CA method reviewed in Section 3, in contrast to Newton's and the Modified Newton methods. They considered the application of the CA method using 2 to 6 vectors of the sequence (8) to obtain the approximate solution (9) of the linear system (4).

In this work, we propose the five *Inexact Combined Approximations* (ICA) strategies described below. All of them rely on the use of the iterative scheme (8) to approximately solve the linear system (4) at each iteration of Newton's method. The strategies differ on the frequency of \mathbf{K}_T factorizations, on the updating scheme for matrix $\Delta\mathbf{K}$ and on the use of (8) for the solution of the adjoint linear system (15) related to the objective function gradient computation. To help future reference, each strategy is identified by its abbreviation.

upK1: \mathbf{K}_T is factored only at the first iteration of Newton's method; $\Delta\mathbf{K}$ is updated at each iteration of Newton's method.

upK1g: same as upK1, with the addition that the linear system (15) is also solved inexactly by means of the iterative scheme (8).

upK100: \mathbf{K}_T is factored only at the first iteration of Newton's method; $\Delta\mathbf{K}$ is updated every 100 iterations of Newton's method.

upK100g: same as upK100, with the addition that the linear system (15) is also solved inexactly by means of the iterative scheme (8).

upK03K100g: \mathbf{K}_T is factored only at every 3 iterations of the SPLP method; $\Delta\mathbf{K}$ is updated every 100 iterations of Newton's method, and the linear system (15) is solved inexactly by means of the iterative scheme (8).

In order to evaluate the performance of the proposed strategies, they are compared with two factorization schemes commonly found in literature:

N (Newton): \mathbf{K}_T is factored at every iteration of Newton’s method.

MN (Modified Newton): \mathbf{K}_T is factored only at the first iteration of Newton’s method.

It is important to mention that, independently of the adopted strategy, in the first five iterations of the SPLP method, Newton’s method is always applied to obtain the approximate solutions of the nonlinear system (2) to reduce the impact of the starting solution on the overall optimization process.

4.3 Implementation Details

The performance of the proposed strategies will be investigated for the four benchmark structures and compliant mechanisms presented in Subsection 4.1.

When we apply an optimization algorithm for solving problem (1), at every iteration we need to solve the nonlinear system (2) in order to compute the objective function. No matter the strategy adopted here, our stopping criterion for Newton’s method is $\|\mathbf{r}(\mathbf{u}^{(\ell)}, \boldsymbol{\rho})\|_\infty \leq 10^{-5}$.

For strategies upK1, upK1g, upK100, upK100g and upK03K100g, in a fixed iteration ℓ of Newton’s method, the linear system (4) is solved inexactly by means of the ICA method described in Section 3. In the solution of this system, we used a stopping criterion based on the value of the relative magnitude of the residual of the linear system (4), given by

$$\widehat{R}_k^{(\ell)} = \frac{\|\mathbf{K}_T \mathbf{s}^{(k)} + \mathbf{r}\|_\infty}{\|\mathbf{r}\|_\infty}, \quad k = 0, 1, 2, \dots$$

where $\mathbf{K}_T \equiv \mathbf{K}_T(\mathbf{u}^{(\ell)}, \boldsymbol{\rho})$ and $\mathbf{r} = \mathbf{r}(\mathbf{u}^{(\ell)}, \boldsymbol{\rho})$. If we get $\widehat{R}_{k^*}^{(\ell)} < \varepsilon_R$ (where ε_R is a small positive constant) for some $k^* \leq 10$, we consider that $\mathbf{s}^{(\ell)} = \mathbf{s}^{(k^*)}$ is a good approximation for the solution of (4). Otherwise, we update the factorization of \mathbf{K}_T , and solve the linear system (4) exactly.

When strategies upK1g, upK100g and upK03K100g are adopted, the ICA method is also applied for inexactly solving the linear system (15). In this case, the relative magnitude of the residual is defined as

$$T_k = \frac{\|\widehat{\mathbf{K}}_T \boldsymbol{\lambda}^{(k)} + \mathbf{l}\|_\infty}{\|\mathbf{l}\|_\infty}, \quad k = 0, 1, 2, \dots,$$

and we require that $T_{\bar{k}} < \varepsilon_T$ for some $\bar{k} \leq 10$. If this criterion is not satisfied, we update the factorization of $\widehat{\mathbf{K}}_T$, and solve the linear system (15) exactly. In our numerical tests, we took $\varepsilon_R = 10^{-2}$ and $\varepsilon_T = 10^{-8}$. A more stringent value is adopted for ε_T in order to guarantee a high level of accuracy in the computation of the derivatives of the objective function.

With the aim of ensuring the global convergence of Newton’s method and avoiding small decreases of $\|\mathbf{r}(\mathbf{u}, \boldsymbol{\rho})\|_2^2$ even with large steps, for all of the strategies we adopt the Armijo’s line search [27]. When dealing with topology optimization problems under geometric nonlinearity, the value of the penalty parameter p of the SIMP method plays a crucial role in the stabilization of the overall optimization process. Based on our previous experience [16], the initial value of p is set to 1.0 and it is increased by $\Delta p = 0.1$ after every 10 iterations of the SPLP method until it reaches 3.0. The minimum value ρ_{\min} allowed for the densities in problem (1) was set to 0.001, to avoid the singularity of the matrix \mathbf{K}_T . The density filter proposed by Bruns and Tortorelli [9] was applied to prevent the checkerboard-like pattern in the optimal distribution of material [14]. In our tests, the number of elements used to define the filter radius were 10, 5, 7.5 and 5, respectively, for the cantilever beam, the slender beam, the inverter and the gripper.

The algorithm presented was coded in C++. The CPLEX 12.1 software library was used for solving the subproblems of the SPLP algorithm, and the linear systems were solved using the

CHOLMOD 1.7 library. All of the tests were performed on a personal computer with an Intel Core i7-6500U processor, under the Ubuntu Linux 16.4 operating system.

5 Performance of the strategies considering a fixed budget

With the aim of providing a fair comparison of the performance of the several strategies proposed here, we have first solved all of the problems with a fixed budget of 300 iterations of the SPLP method. The tables presented in this and in the following sections contain the value reached for the objective function $F(\boldsymbol{\rho})$, the accumulated number of iterations of Newton's method and the total time spent to achieve the optimal solution and to evaluate $F(\boldsymbol{\rho})$, that is composed by the sum of the time consumed for assembling \mathbf{K}_T and its factorization, in the assembling of the right-hand side (RHS) vectors, and in the solution of the linear systems (4) and (15). Moreover, the tables show the time spent for solving the SPLP subproblems, for applying the filter to the densities, and for computing the gradient vector $\nabla F(\boldsymbol{\rho})$. We remark that the CPU times are always expressed in seconds.

Table 1: Results obtained for 300 iterations of SPLP (cantilever beam and slender beam).

Cantilever beam 400 × 100	N	MN	upK1	upK1g	upK100	upK100g	upK03 K100g
$F(\boldsymbol{\rho})$ - value	2036.42	2036.62	2036.42	2036.57	2036.62	2036.57	2036.49
# Newton iter.	679	1147	826	814	839	814	904
CPU time (s)							
Total	1579.93	1210.52	1208.69	1029.80	1150.91	986.30	732.38
$F(\boldsymbol{\rho})$	1218.75	868.40	847.89	688.44	801.32	637.12	373.62
\mathbf{K}_T	181.18	184.92	197.34	199.15	145.51	148.82	95.27
RHS	25.37	37.25	32.55	39.17	32.69	39.34	56.28
Factorizations	1000.31	628.47	597.50	415.95	602.27	414.50	161.29
Linear systems	11.89	17.76	20.50	34.17	20.85	34.46	60.79
$\nabla F(\boldsymbol{\rho})$	104.95	102.12	105.70	102.45	106.19	107.59	104.99
SPLP solving	159.17	145.15	158.65	143.24	146.34	143.54	155.87
Filtering	90.76	88.78	90.23	89.47	90.87	91.75	91.82
Other	6.30	6.07	6.22	6.20	6.20	6.30	6.08
Slender beam 600 × 75	N	MN	upK1	upK1g	upK100	upK100g	upK03 K100g
$F(\boldsymbol{\rho})$ - value	138.62	138.52	138.68	138.77	138.68	138.77	138.62
# Newton iter.	648	758	658	667	658	670	838
CPU time (s)							
Total	1622.93	1262.76	1293.72	1201.68	1263.94	1170.56	876.84
$F(\boldsymbol{\rho})$	1208.74	853.88	878.07	770.80	846.39	741.24	463.44
\mathbf{K}_T	189.38	210.10	191.42	199.88	157.05	162.87	106.44
RHS	26.97	30.74	29.07	43.71	29.01	46.34	59.35
Factorizations	979.93	599.03	640.57	480.06	643.33	479.84	232.96
Linear systems	12.46	14.01	17.01	47.15	17.00	52.19	64.69
$\nabla F(\boldsymbol{\rho})$	34.74	35.33	35.09	35.12	35.06	35.37	35.35
SPLP solving	351.85	345.64	352.93	367.64	354.74	365.88	350.45
Filtering	25.71	25.97	25.73	26.23	25.86	26.16	25.69
Other	1.89	1.94	1.90	1.89	1.89	1.91	1.91

From Table 1, one may notice that the optimal values of the objective function among the strategies are very similar for the cantilever beam and for the slender beam. With Newton’s method, the evaluation of the objective function takes 77.1% of the total time demanded for solving the problem for the cantilever beam, and 74.5% for the slender beam. This percentage is substantially reduced if the `upK03K100g` strategy is adopted. From the total time spent to obtain the optimal structure, the computation of $F(\boldsymbol{\rho})$ consumes 51.0% for the cantilever beam, and 52.9% for the slender beam.

A slight reduction on the time consumed to assemble \mathbf{K}_T is noted if `upK100` is adopted, in comparison with the `upK1` strategy. For these two strategies, and for both structures, the time spent on the factorization of \mathbf{K}_T remains very similar. On the other hand, with the adoption of the strategies `upK1g` and `upK100g`, we observe a significant reduction of the time spent in the factorization of \mathbf{K}_T as compared with the counterparts `upK1` and `upK100` – about 30% for the cantilever beam, and 25% for the slender beam.

As we relax the proposed strategies, it is noticeable the decreasing of the demanded time for computing the objective function, and consequently, for solving the problem. Indeed, all of the five ICA strategies outperformed the original and the modified Newton methods. For the cantilever beam, the reduction attained on the time spent to evaluate $F(\boldsymbol{\rho})$ by strategies `upK1`, `upK1g`, `upK100` and `upK100g`, in comparison with Newton’s method, is of 30.4%, 43.5%, 34.3% and 47.7%, respectively. The reduction is even more pronounced if we consider the `upK03K100g` strategy, reaching 69.3% for this structure. When it comes to the slender beam, similar percentage reductions have been achieved, namely 27.4%, 36.2%, 30.0%, 38.7%, and 61.7% for strategies `upK1`, `upK1g`, `upK100`, `upK100g`, and `upK03K100g`, respectively.

To put the effect of the geometric nonlinearity in perspective, we have also considered the two structures as described in Section 4.1, but using the *linear elastic* assumption to define the stiffness matrix, so that it varies just with the densities, and do not depend on the displacements any longer. Adopting the policy of factoring such a matrix at every call of the objective function, i.e. the *original* strategy analyzed in [28], we have solved the corresponding topology optimization problem, reaching the so-called *small displacement* configuration. Fig. 3 depicts the optimal topologies, with small and large displacements, for the cantilever beam and the slender beam, respectively. For the cantilever beam, it is evident the lack of symmetry about the medium horizontal line presented by the structure under large displacements, to cope with the nonlinear requirement, as compared with the structure under small displacements. When it comes to the slender beam, it is also significant the effect of the geometric nonlinearity upon the optimal configuration. It must be stressed that the structures obtained for the seven strategies presented on Table 1 are quite similar, so only the results for the `upK100g` strategy are shown.

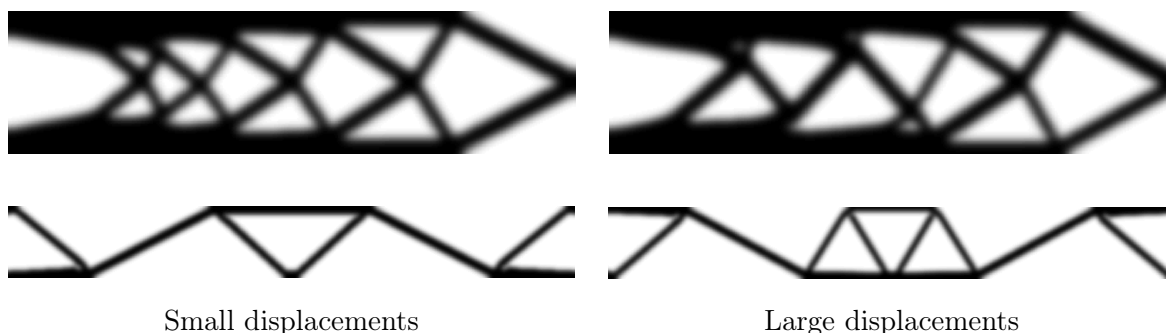


Figure 3: Optimal topologies for the cantilever beam 400×100 (top) and the slender beam 600×75 (bottom).

Figure 4 shows the time consumed by each strategy to evaluate the objective function, and the number of iterations performed by Newton’s method at each iteration of the SPLP method, together with the maximum number of iterations performed by the iterative scheme (8) to ap-

proximately solve the linear system (4), for the cantilever beam.

We can observe from Fig. 4 that, if Newton’s method is employed, it takes at most 3 iterations to reach the approximate solution of the nonlinear system (2), but, due to the expensive iterations, the average time spent to compute the objective function is about 4.0 seconds. With the adoption of the Modified Newton method, we can note a good decrease in this average time as compared with Newton’s method (it oscillates between 2.5 and 3.0 seconds), but a slower convergence is experienced in some occasions. For example, at the iteration 210 of the SPLP method, 10 iterations were necessary to obtain the approximate solution of (2). This behavior can be explained by the fact that, for the Modified Newton method, the matrix \mathbf{K}_T is factored only at the initial point, without carrying any information about the changes of \mathbf{K}_T along the iterative process.

The upK1 strategy represents an enhancement of the Modified Newton method, since the iterative scheme (8) takes into account the variations on \mathbf{K}_T by means of the matrix $\Delta\mathbf{K}$. This is reflected in the expressive acceleration in the convergence of such inexact Newton method, as we can see in Fig. 4. Moreover, in almost all of the callings of this inexact Newton method, the approximate solution of the linear system (4) with the desired precision was obtained already with the first term of the sequence (8). Despite of these facts, the time consumed to evaluate $F(\boldsymbol{\rho})$ by the Modified Newton method and by strategy upK1 are quite similar. On the other hand, strategy upK1g showed a noticeable reduction in the time spent to compute $F(\boldsymbol{\rho})$ in comparison with upK1, since it does not require the factorization of \mathbf{K}_T for the solution of the adjoint linear system (15). Moreover, we observed the fast convergence of this inexact Newton method. According to Fig. 4, the average time consumed to compute $F(\boldsymbol{\rho})$ is about 2.2 seconds when strategy upK1g is applied, a reduction of 43,5 % when compared to Newton’s method.

When the upK100 strategy is employed, a 26.2 % reduction is attained in the time spent to assemble \mathbf{K}_T , as compared with upK1. The decrease reached in this step by upK100g is of 25.3 % in comparison with upK1g. Strategies upK1g and upK100g required much less time to evaluate $F(\boldsymbol{\rho})$ compared to Newton’s method, showing a reduction of 43.5 % and 47.8 %, respectively.

The adoption of strategy upK03K100g produced the most remarkable improvement in the time spent to evaluate the objective function, in relation to Newton’s method. As we can see in Fig. 4, in most of the iterations, the evaluation of $F(\boldsymbol{\rho})$ demanded less than 1.5 seconds, requiring less than 1 second in many cases, while Newton’s method spent about 4 seconds to compute the same function. It should be mentioned that the maximum number of iterations of the iterative scheme (8) can be reached when we are far from the solution, due to the lack of information on the changes of the factorization of \mathbf{K}_T . Whenever this happens, the factorization of \mathbf{K}_T is updated, and we solve the full linear system (4). Fortunately, this rarely occurs, so the speed of convergence of the inexact Newton method is almost not affected. According to Table 1, strategy upK03K100g requires 41.4 % less time than upK100g to compute $F(\boldsymbol{\rho})$. This reduction increases to 69.3 % when the comparison is made with Newton’s method. Taking also into account the decreasing in the time spent with the factorization of \mathbf{K}_T , the reduction are even more noticeable, reaching 61.1 % and 83.9 % when compared to the upK100g strategy and Newton’s method, respectively. Now, we will discuss the results obtained for the inverter and for the gripper mechanisms, considering the fixed budget of 300 iterations of the SPLP method. These results are summarized on Table 2. One may notice that the maximum variation between the optimal values of the objective function was of 0.09 % for the inverter and of 0.26 % for the gripper, which is very reasonable from the practical point of view. As expected, when Newton’s method is employed, the factorization of \mathbf{K}_T takes most of the total time for solving the problems. In fact, the factorization of \mathbf{K}_T consumes 90 % and 86.5 % of the total time for the inverter and for the gripper, respectively. When the upK03K100g strategy is adopted, these values are reduced to 41.1 % and 35.9 % for the inverter and the gripper, respectively.

Analogously to the results achieved for the rigid structures, the reductions attained in the time spent to compute $F(\boldsymbol{\rho})$ are remarkable. Besides, upK03K100g is much cheaper than the

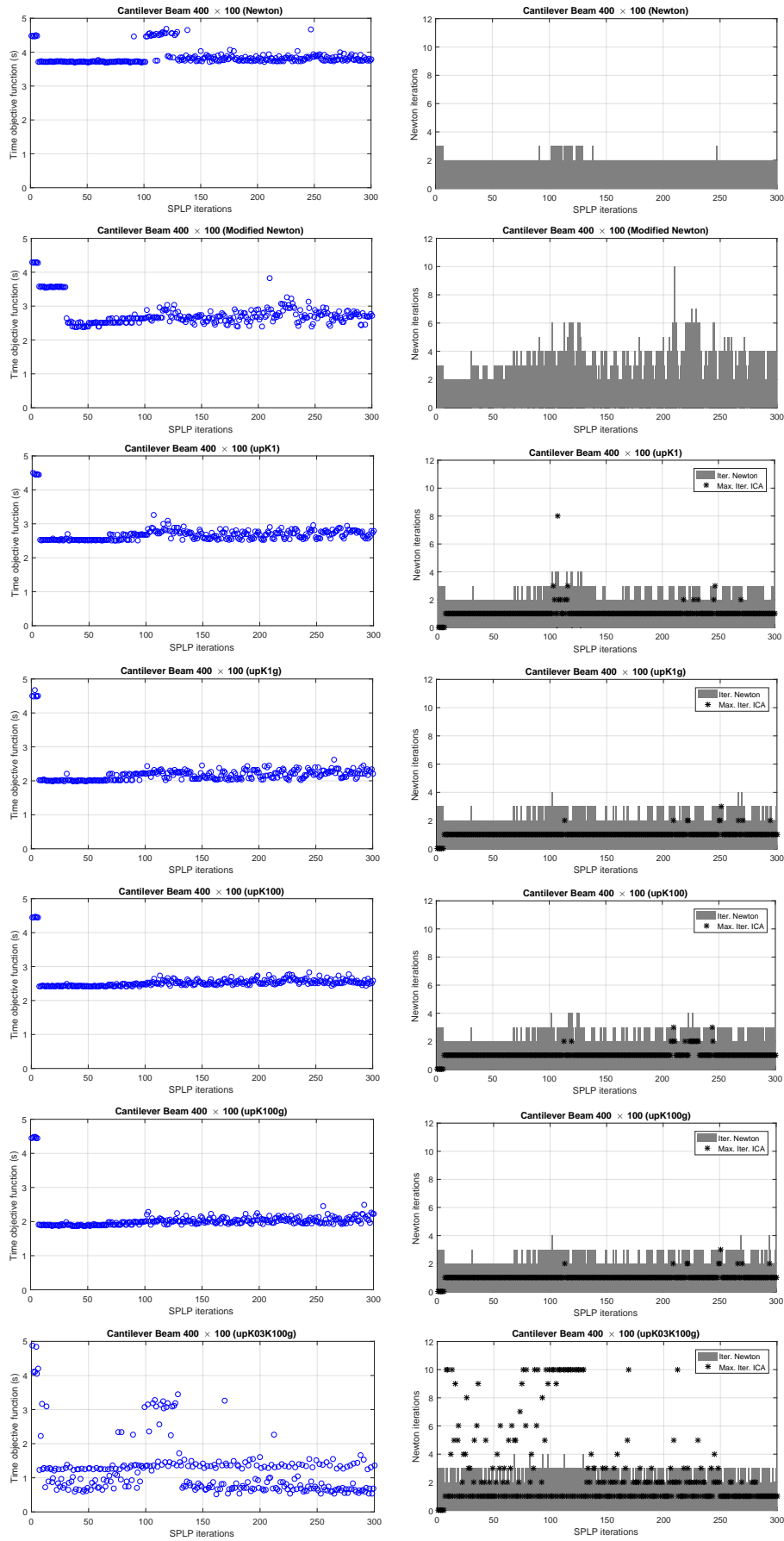


Figure 4: Time spent to compute the objective function (left) and number of iterations of Newton's Method (right) in the solution of the cantilever beam (400×100).

Table 2: Results obtained for 300 iterations of SPLP (Inverter and Gripper).

Inverter 300 × 150	N	MN	upK1	upK1g	upK100	upK100g	upK03 K100g
$F(\boldsymbol{\rho})$ - value	-8.6969	-8.6989	-8.7020	-8.7035	-8.6997	-8.7028	-8.7046
# Newton iter.	696	1065	859	849	848	841	929
CPU time (s)							
Total	1883.89	1334.16	1344.36	1097.37	1293.52	1066.04	756.60
$F(\boldsymbol{\rho})$	1691.98	1144.86	1149.91	905.20	1102.38	860.02	564.05
\mathbf{K}_T	161.20	194.80	178.60	179.35	128.35	132.06	106.75
RHS	28.87	38.90	42.83	54.16	42.22	54.37	66.69
Factorizations	1487.78	891.76	895.51	614.71	899.80	616.35	310.82
Linear systems	14.13	19.40	32.97	56.98	31.98	57.24	79.79
$\nabla F(\boldsymbol{\rho})$	35.44	36.17	37.69	36.37	36.27	36.61	36.57
SPLP solving	128.50	124.56	126.68	126.87	126.22	140.25	127.22
Filtering	26.23	26.77	28.17	27.09	26.88	27.29	26.90
Other	1.74	1.80	1.91	1.84	1.77	1.87	1.86
Gripper 320 × 160	N	MN	upK1	upK1g	upK100	upK100g	upK03 K100g
$F(\boldsymbol{\rho})$ - value	-3.8481	-3.8478	-3.8556	-3.8493	-3.8577	-3.8487	-3.8460
# Newton iter.	659	888	732	725	732	744	864
CPU time (s)							
Total	2530.57	1828.94	1817.90	1488.72	1766.46	1437.66	999.59
$F(\boldsymbol{\rho})$	2188.84	1485.33	1477.07	1143.88	1425.90	1090.35	650.17
\mathbf{K}_T	208.06	237.01	218.70	222.47	169.91	174.48	128.89
RHS	32.40	39.31	41.90	52.61	42.26	53.62	72.89
Factorizations	1932.43	1189.14	1186.75	816.90	1183.57	809.60	358.68
Linear systems	15.95	19.87	29.72	51.48	30.16	52.65	89.71
$\nabla F(\boldsymbol{\rho})$	102.56	104.83	103.80	106.30	104.30	106.54	108.18
SPLP solving	147.57	145.99	145.25	145.73	144.11	147.71	148.28
Filtering	85.64	86.76	85.83	86.43	86.19	86.64	86.44
Other	5.96	6.03	5.95	6.38	5.96	6.42	6.52

other strategies. As an example, for the inverter, strategies upK1, upK1g, upK100, upK100g and upK03K100g spent, respectively, 32.0 %, 46.5 %, 34.8 %, 49.2 % and 66.7 % less time to evaluate $F(\boldsymbol{\rho})$ in comparison with Newton’s method.

Aiming to assess the effect of the geometric nonlinearity for the mechanisms, following the same ideas applied to the structures, we have also generated the optimal configurations under small displacements for the inverter and the gripper, so they can be compared with the optimal configurations obtained when large displacements are considered. The varied topologies obtained are presented in Fig. 5. Since there was no significant difference between the structures obtained with the strategies presented on Table 2, only the results for the upK100g strategy are shown.

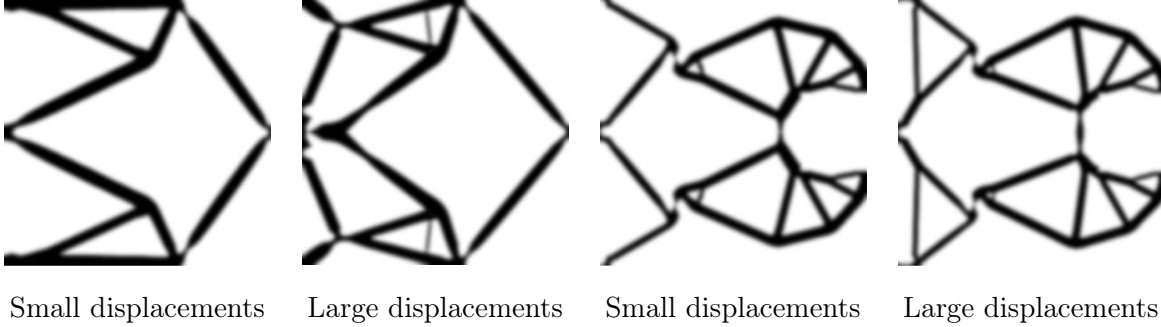


Figure 5: Optimal topologies for the inverter 300×150 (left) and the gripper 320×160 (right).

Figure 6 shows the time spent by each strategy to compute $F(\boldsymbol{\rho})$ and the number of iterations performed by Newton’s method at each iteration of the SPLP method, along with the maximum number of iterations required to approximately solve the linear system (4) for the gripper mechanism. As we can see, the convergence of Newton’s method is very fast. In fact, in almost all of the iterations of the SPLP method, the approximate solution of the nonlinear system (2) was found in just 2 iterations. On the other hand, the average time spent to compute $F(\boldsymbol{\rho})$ is equal to 7.0 seconds. With the adoption of the Modified Newton method, we can observe that, at the tenth iteration of the SPLP method, 13 iterations were necessary to find the approximate solution of the nonlinear system (2), but, in general, $F(\boldsymbol{\rho})$ is computed in no more than 5.5 seconds.

The overall performance of the Modified Newton method and of strategies upK1 and upK100 were very similar, but the last two strategies required less iterations for solving the nonlinear system (2), due to the frequent updating of the $\Delta\mathbf{K}$ matrix. Moreover, in most cases, the approximate solution of the linear system (4) was found in no more than 3 iterations of the scheme described in (8). Despite of similarities between strategies upK1 and upK100, the latter spent 22.3 % less time to assemble \mathbf{K}_T than the former.

Strategies upK1g and upK100g required much less time to factorize \mathbf{K}_T than its counterparts upK1 and upK100. In fact, for the two compliant mechanisms, upK1g spent 31.3 % less time than upK1. The same amount of reduction was attained by the upK100g strategy in comparison with upK100. We also observe in Fig. 6 that the convergence of the inexact Newton variants have similar overall behavior.

At the iterations of the SPLP method in which the factorization of \mathbf{K}_T was reused, the upK03K100g strategy took no more than 2 seconds to compute $F(\boldsymbol{\rho})$. In some occasions, the time spent was less than 1 second. Because of the smaller frequency of factorizations of \mathbf{K}_T , the average number of iterations to obtain the solution of the linear system (4) was larger than those required by the other inexact Newton strategies. Despite this fact, the accuracy of the approximate solutions of the linear system (4) and of the nonlinear system (2) were not spoiled. For the gripper mechanism, this strategy took 70.3 % less time than Newton’s method to compute $F(\boldsymbol{\rho})$, and the reduction of the time consumed in the factorization of \mathbf{K}_T reached 81.4 %.

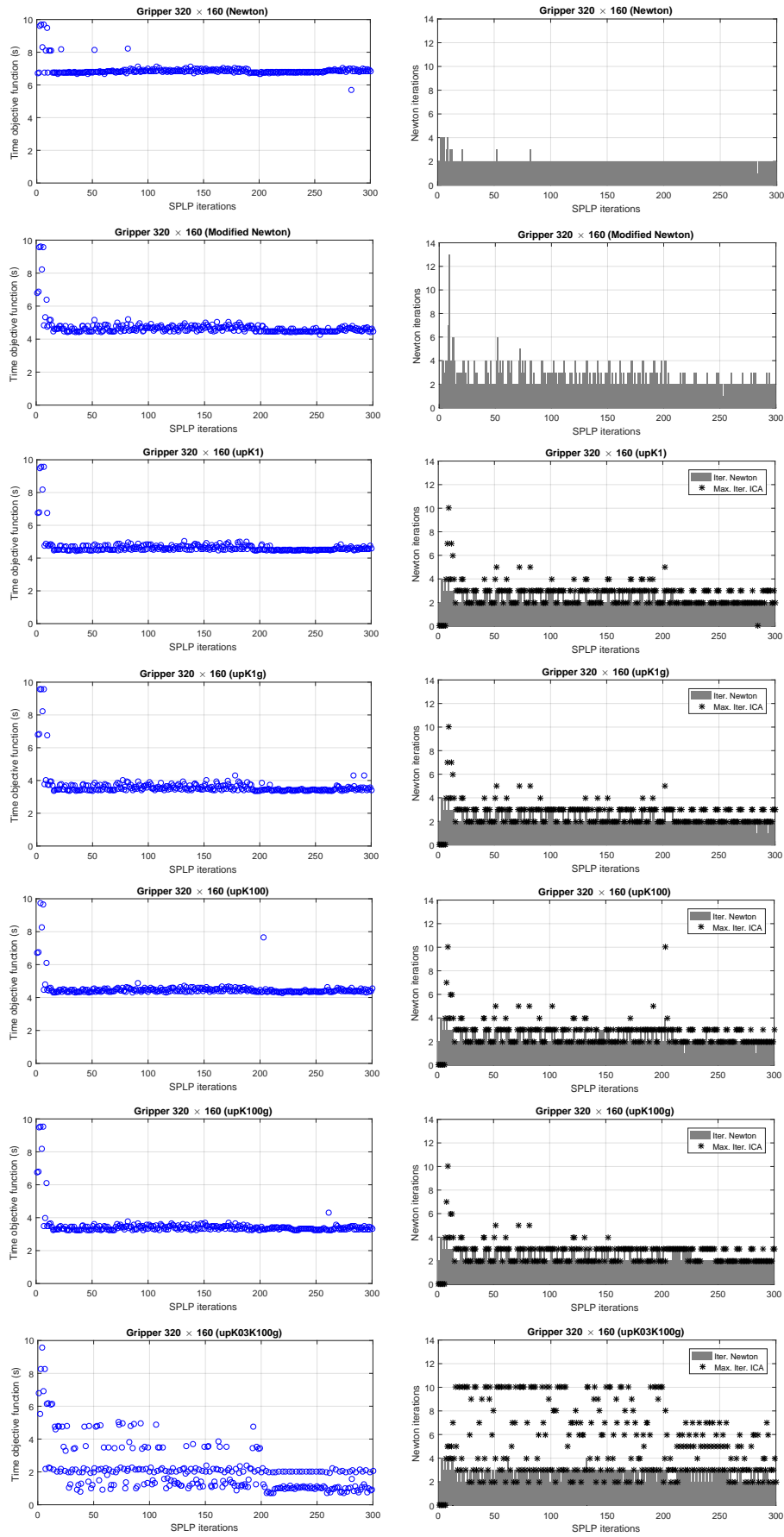


Figure 6: Time spent to compute the objective function (left) and number of iterations for Newton's Method (right) in the solution of the gripper (320×160).

6 Effect of mesh refinement

The time consumed to evaluate the objective function (and, consequently, the total time spent for solving the topology optimization problem) is directly influenced by the mesh refinement of the design domain. To investigate the impact of the number of finite elements on the time spent to compute $F(\boldsymbol{\rho})$, we chose four different meshes for the slender beam and for the inverter, considering a fixed budget of 300 iterations of the SPLP method. For the slender beam, the design domain was discretized into $200 \times 25 = 5000$, $400 \times 50 = 20000$, $600 \times 75 = 45000$ and $800 \times 100 = 80000$ elements. In each case, the filter radius was defined accordingly, corresponding to the length of 2.5, 5.0, 7.5 and 10.0 elements, respectively. The upper half of the design domain of the inverter was discretized into $200 \times 100 = 20000$, $300 \times 150 = 45000$, $400 \times 200 = 80000$ and $500 \times 250 = 125000$ elements, and the filter radius was set to the length of 5.0, 7.5, 10.0 and 12.5 elements, respectively. The tables that show how the performance of each strategy was affected by the mesh refinement are available in Appendix A.

6.1 Slender beam

First of all, it is worth mentioning that, for all of the meshes considered, the value of $F(\boldsymbol{\rho})$ attained after 300 iterations of the SPLP method differ very little regardless of the strategy adopted, corroborating the robustness of the reanalysis strategies proposed here. Since the optimal topologies are also very similar among strategies, only the results related to the upK100g strategy are shown in Fig. 7.

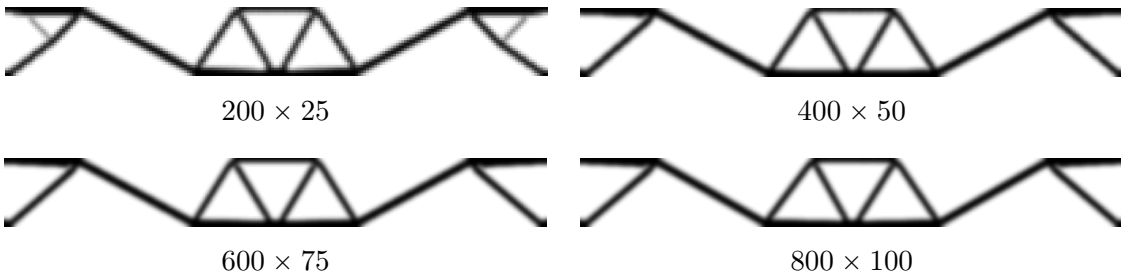


Figure 7: Optimal topologies for the slender beam.

Figure 8, however, shows that the time required to evaluate the objective function may vary significantly among strategies. This figure suggest that, for all of the methods, there is an almost linear relation between the time spent to compute $F(\boldsymbol{\rho})$ and the product of the size of matrix \mathbf{K}_T and its bandwidth. Moreover, all of our strategies not only provide a considerable decrease on the overall time spent to compute $F(\boldsymbol{\rho})$ but also this reduction become more evident as we refine the design domain. In fact, the slopes of the regression lines of the Modified Newton method and strategies upK1, upK1g, upK100, upK100g and upK03K100g are, respectively, 30.2%, 33.2%, 44.4%, 35.0%, 48.7% and 66.3% smaller than the slope of the line associated with Newton's method.

Figure 9 shows the percentage of decrease in the time spent to evaluate $F(\boldsymbol{\rho})$ with respect to Newton's method, for the four discretizations considered for the slender beam. For the coarsest mesh, the Modified Newton method took almost twice the number of iterations of Newton's method, resulting in an increase of 5.7% in the time spent to compute the objective function. For the remaining discretizations, the performance of the Modified Newton method and strategy upK1 were very similar, although the latter took fewer iterations due to its frequent updating of $\Delta\mathbf{K}$. It is clear from the figure that the inexact solution of the system related to the objective function gradient becomes more relevant as the mesh gets finer, so the decrease in time is more pronounced for the upK1g, upK100g and upK03K100g strategies.

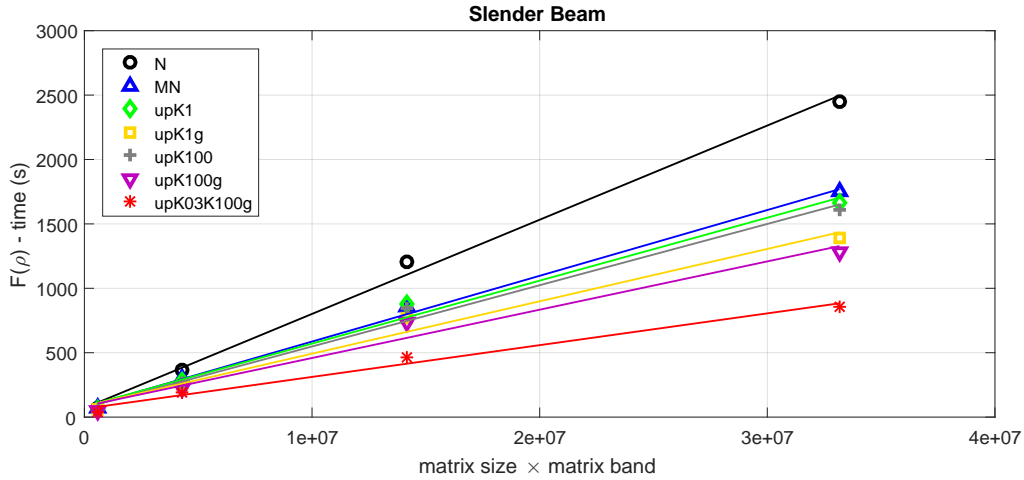


Figure 8: $F(\rho)$ -time for each strategy according to the dimension of \mathbf{K}_T (slender beam).

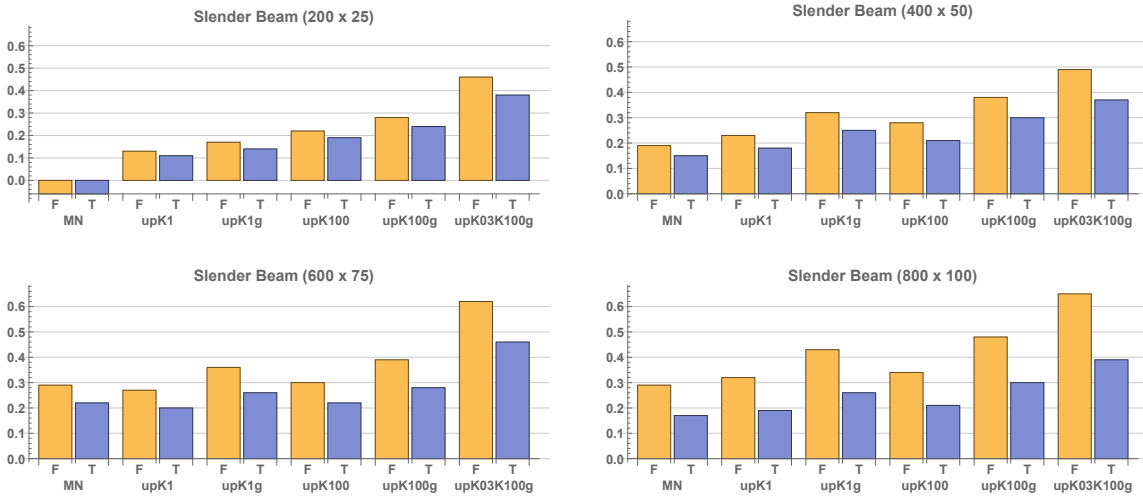


Figure 9: Percentage of decrease in the time demanded to evaluate the objective function (F) and in the total time (T), as compared with Newton's method, for the slender beam.

Although strategies `upK1g` and `upK100g` attained an average reduction of 34.2% and 38.5%, respectively, for the last two discretizations, `upK03K100g` showed the best figures for all of the meshes, as expected. For this strategy, the reduction of the time consumed in evaluating $F(\boldsymbol{\rho})$ varied from 46.0% to 65.0%. When it comes to the time for assembling \mathbf{K}_T , the reduction ranged between 38.4% and 45.0%, while the factorization of \mathbf{K}_T showed an even more significant result, with a reduction in the range 71.6% to 77.4%.

Figure 9 also shows the percentage of decrease in the total time spent by the inexact Newton strategies, with respect to Newton’s method. The difference between the two percentages presented for each strategy reveals the relevance of the remained steps performed at each iteration of the SPLP method. In short, for the Modified Newton method and strategies `upK1` and `upK100`, the decrease in the time spent to obtain the optimal topologies was, in average, 18.1%, 19.3% and 21.4%, respectively. When strategies `upK1g` and `upK100g` were adopted, an average decrease of 25.6% and 29.5% was obtained. Finally, the `upK03K100g` strategy showed an average decrease of 40.0%.

6.2 Inverter

As we observed for the slender beam, for all of the mesh sizes, the value of the objective function attained by the various strategies after 300 iterations of the SPLP method was almost the same. In this case, the difference did not exceed 0.07%, which is very reasonable from the practical point of view. Moreover, the number of iterations necessary to obtain the approximate solution of the nonlinear system (2) also showed little variation among strategies. As a consequence, the optimal topologies obtained were quite similar, so only the results for the `upK100g` strategy are shown in Fig. 10.

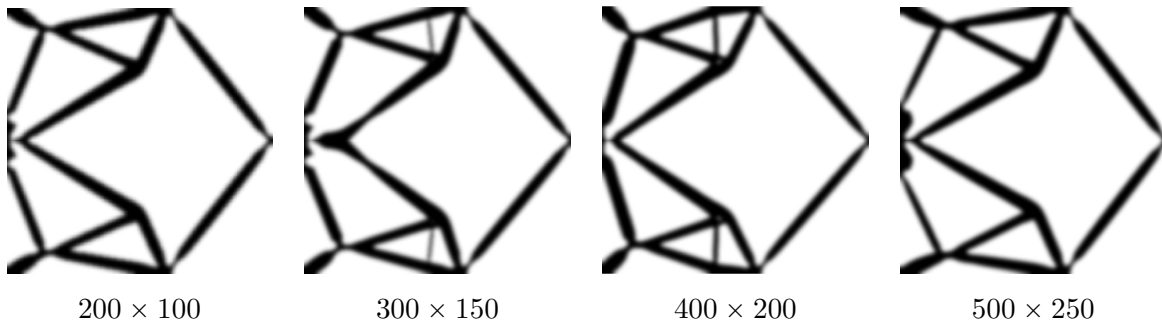


Figure 10: Optimal topologies for the inverter.

Figure 11 shows how the time spent to compute $F(\boldsymbol{\rho})$ depends on the problem size. Once again, we observe that our strategies are very efficient in reducing the time consumed in computing $F(\boldsymbol{\rho})$ as the mesh is refined. The regression lines suggest that the growth rates of the Modified Newton method and strategies `upK1` and `upK100` are very similar. The same occurs with `upK1g` and `upK100g`. As expected, the `upK03K100g` strategy achieved the best performance. Compared to the regression line of Newton’s method, the lines of the Modified Newton method and strategies `upK1` and `upK100` showed a 37% smaller slope. For strategies `upK1g` and `upK100g`, the slope is 54.1% smaller, and for `upK03K100g` the reduction is about 72.0%.

Figure 12 presents the percentage of decrease in the time spent to evaluate $F(\boldsymbol{\rho})$ and in the overall time of the algorithm, with respect to Newton’s method. From the figure, one can notice that the percentages provided by the Modified Newton method and strategies `upK1` and `upK100` are very similar, ranging from 31.0% to 37.0% when we take into account the four mesh sizes. Analogously to the results shown in Fig. 9, the adoption of the iterative scheme (8) to obtain an approximate solution for the adjoint system (15) resulted in a substantial reduction in the time spent with the reanalysis process. In fact, strategies `upK1g` and `upK100g` provided an average

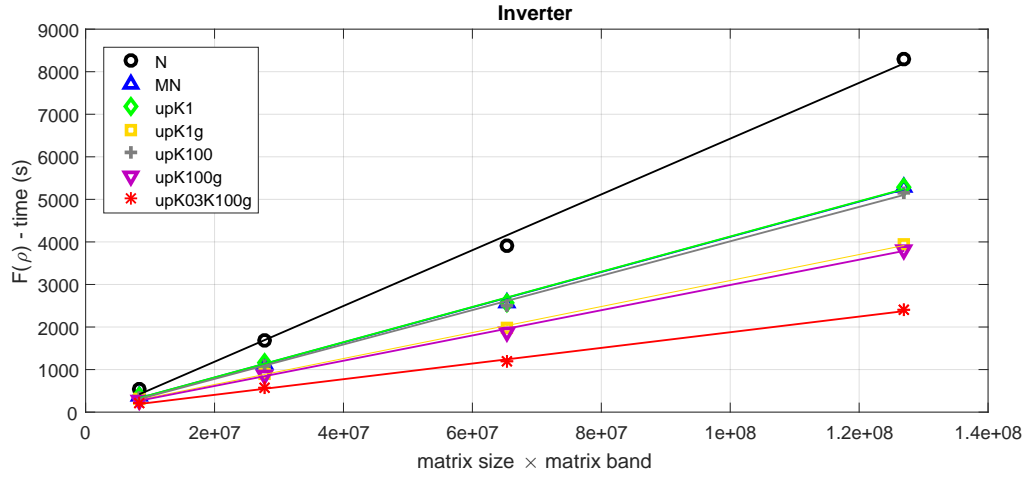


Figure 11: $F(\rho)$ -time for each strategy according to the dimension of \mathbf{K}_T (inverter).

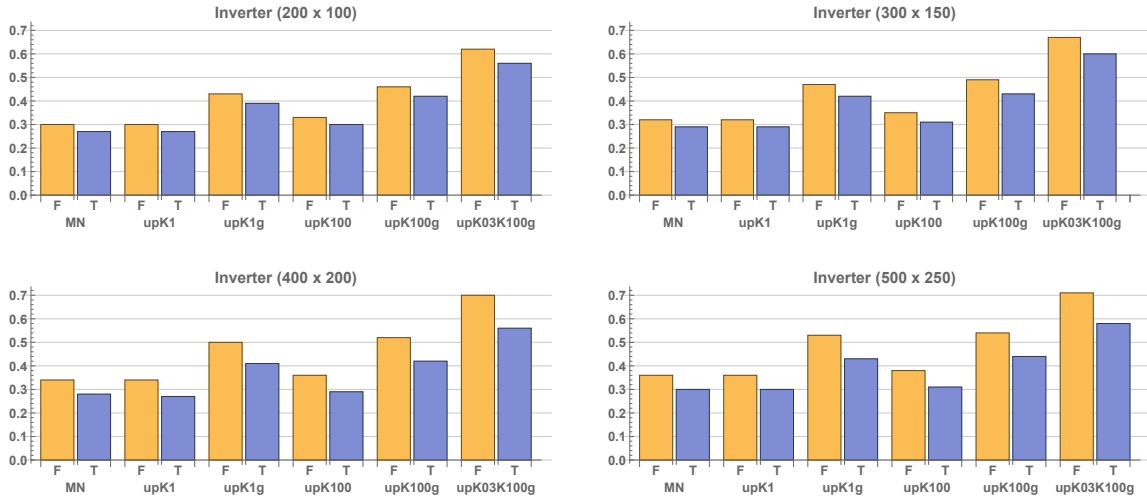


Figure 12: Percentage of decrease in the time demanded to evaluate the objective function (F) and in the total time (T), as compared with Newton's method, for the inverter mechanism.

decrease that ranged from 44.5 % (for the 200×100 mesh) to 53.3 % (for the 500×250 one). As before, strategy **upK03K100g** showed the best results for all of the meshes considered, providing a reduction that varies from 62.2 % (for the coarser mesh) to 71.2 % (for the finer one). On average, this strategy spent 46.0 % less time to assemble \mathbf{K}_T and 78.7 % less time to factorize this matrix, in comparison with Newton’s method.

For the Modified Newton method and strategies **upK1** and **upK100**, the overall time spent by the SPLP algorithm was 28.6 %, 28.1 % and 30.4 % smaller, respectively, than the time consumed when Newton’s method was adopted. For strategies **upK1g** and **upK100g**, we have observed a reduction of 41.0 % and 42.8 %, respectively. Finally, the **upK03K100g** strategy showed an average decrease of 57.4 %.

7 Performance of the SPLP method with the nonlinear reanalysis

In this section, we investigate the performance of the reanalysis strategies when the SPLP method is run until convergence. We have seen above that, for a fixed budget of 300 iterations, these strategies can substantially reduce the overall time spent by the algorithm, as compared to Newton’s method. Our purpose now is to check if this also happens when we adopt a mathematically well founded stopping criterion, as described below.

The Lagrangian function associated with the topology optimization problem is defined by

$$\mathcal{L}(\boldsymbol{\rho}, \theta) := F(\boldsymbol{\rho}) + \theta V(\boldsymbol{\rho}),$$

where $F(\boldsymbol{\rho})$ is the objective function, $V(\boldsymbol{\rho})$ is the volume constraint, and $\theta \in \mathbb{R}$ is the Lagrange multiplier associated with this constraint. Denoting the gradient vector of the Lagrangian function by $\nabla_{\boldsymbol{\rho}}\mathcal{L}(\boldsymbol{\rho}, \theta)$ and defining $v(\boldsymbol{\rho}, \theta) := \boldsymbol{\rho} - \nabla_{\boldsymbol{\rho}}\mathcal{L}(\boldsymbol{\rho}, \theta)$, the continuous projected gradient onto the set

$$X := \{\boldsymbol{\rho} \in \mathbb{R}^{n_{el}} \mid \rho_{\min} \leq \rho_i \leq 1, \quad i = 1, \dots, n_{el}\}$$

is given by $g_P(\boldsymbol{\rho}, \theta) = P_X(v(\boldsymbol{\rho}, \theta)) - \boldsymbol{\rho}$, where $P_X(v(\boldsymbol{\rho}, \theta))$ is the orthogonal projection of the vector $v(\boldsymbol{\rho}, \theta)$ onto X . We consider that the SPLP algorithm has found a good approximation for a stationary point for the topology optimization problem whenever

$$\|g_P(\boldsymbol{\rho}^{(k_s)}, \theta^{(k_s)})\|_{\infty} < 10^{-3}, \quad (16)$$

where $\|\cdot\|_{\infty}$ denotes the max-norm, and $\theta^{(k_s)}$ is the approximate Lagrange multiplier of the volume constraint at the k_s -th iteration of the SPLP algorithm.

The results obtained for the rigid structures and compliant mechanisms using the criterion (16) are shown in Tables 3 and 4, respectively. As we observe, no matter the problem, the optimal values of the objective function at the solution were very similar among strategies. On the other hand, with the exception of the gripper, the number of iterations of the SPLP algorithm showed some variation, affecting the overall performance of the algorithm.

The performance of the various strategies was also affected by the number of iterations required for solving the nonlinear system (2). For the slender beam, for example, most of the strategies took more iterations than Newton’s method, so the decrease in the total CPU time was less noticeable. An exception to this rule, however, is seen when **upK03K100g** is applied to the gripper. In this case, the total time was reduced by more than 60 %, if compared to Newton’s method, even though the number of iterations was 31 % higher.

Figure 13 summarizes the differences observed on the time the various strategies spent to compute the objective function, both for the fixed budget of 300 iterations and in the case we require full convergence. The bars of the figure show the reduction provided by each strategy, with respect to Newton’s method. From the figure, it is easy to notice that, for the cantilever beam and the inverter, the results obtained when we use the stopping criterion (16) are better than those

Table 3: Results obtained using the SPLP stopping criterion (cantilever and slender beams).

Cantilever beam 400 × 100	N	MN	upK1	upK1g	upK100	upK100g	upK03 K100g
$F(\boldsymbol{\rho})$ - value	2019.60	2020.10	2020.01	2019.91	2020.10	2019.91	2020.04
# SPLP iter.	1378	1061	1237	1303	1079	1303	1100
# Newton iter.	2846	3565	3032	2832	2721	3172	2839
CPU time (s)							
Total	6242.60	3670.59	4216.19	3777.00	3570.34	3623.42	1919.11
$F(\boldsymbol{\rho})$	5025.19	2759.84	3102.30	2593.31	2592.30	2430.46	911.78
\mathbf{K}_T	658.27	587.72	639.92	672.96	419.56	512.51	269.09
RHS	106.94	116.85	118.00	153.81	106.00	154.65	156.64
Factorizations	4209.96	1999.73	2270.70	1630.75	1999.47	1626.52	331.50
Linear systems	50.02	55.54	73.68	135.79	67.27	136.78	154.55
$\nabla F(\boldsymbol{\rho})$	420.00	306.87	383.42	417.06	338.85	423.35	343.47
SPLP solving	426.90	335.56	391.65	397.67	340.59	396.76	358.62
Filtering	362.58	260.98	330.89	360.98	291.09	364.73	297.84
Other	7.93	7.34	7.93	7.98	7.51	8.12	7.40
Slender beam 600 × 75	N	MN	upK1	upK1g	upK100	upK100g	upK03 K100g
$F(\boldsymbol{\rho})$ - value	137.67	137.64	137.66	137.61	137.66	137.61	137.67
# SPLP iter.	541	625	686	625	686	625	541
# Newton iter.	1130	1399	1424	1317	1424	1320	1448
CPU time (s)							
Total	2613.13	2217.55	2452.18	2078.82	2491.74	1929.06	1181.73
$F(\boldsymbol{\rho})$	2081.28	1651.55	1847.23	1471.68	1871.53	1337.04	647.42
\mathbf{K}_T	303.87	363.87	378.22	374.06	318.36	291.11	164.61
RHS	47.29	58.03	64.01	81.30	66.25	80.72	94.82
Factorizations	1708.34	1203.17	1367.30	942.58	1447.84	888.14	290.56
Linear systems	21.78	26.48	37.70	73.74	39.08	77.07	97.43
$\nabla F(\boldsymbol{\rho})$ s	60.66	70.76	77.47	73.39	79.77	71.44	62.05
SPLP solvings	424.32	440.87	468.25	477.47	479.31	465.33	424.79
Filterings	44.78	52.06	56.95	54.02	58.84	52.98	45.36
Others	2.09	2.31	2.28	2.26	2.29	2.27	2.11

Table 4: Results obtained using the SPLP stopping criterion (Inverter and Gripper).

Inverter 300 × 150	N	MN	upK1	upK1g	upK100	upK100g	upK03 K100g
$F(\boldsymbol{\rho})$ - value	-8.7438	-8.7276	-8.7020	-8.7278	-8.7221	-8.7337	-8.7248
# SPLP iter.	439	367	325	351	350	382	342
# Newton iter.	835	1236	929	967	971	1039	1033
CPU time (s)							
Total	2660.33	1592.05	1452.41	1258.17	1482.75	1311.61	821.47
$F(\boldsymbol{\rho})$	2409.59	1374.04	1246.94	1044.12	1270.01	1070.33	610.67
\mathbf{K}_T	236.58	230.54	193.87	209.72	148.21	169.34	117.72
RHS	40.89	45.46	46.21	61.54	48.01	66.47	73.94
Factorizations	2112.25	1075.41	971.24	708.80	1037.80	765.76	330.75
Linear systems	19.87	22.63	35.62	64.06	35.99	68.76	88.26
$\nabla F(\boldsymbol{\rho})$	51.00	43.70	40.62	42.09	42.01	45.88	41.45
SPLP solving	160.26	140.06	132.53	138.58	137.77	158.82	136.88
Filtering	37.62	32.34	30.31	31.44	31.09	34.60	30.51
Other	1.86	1.91	2.01	1.94	1.87	1.98	1.96
Gripper 320 × 160	N	MN	upK1	upK1g	upK100	upK100g	upK03 K100g
$F(\boldsymbol{\rho})$ - value	-3.8542	-3.8504	-3.8567	-3.8546	-3.8596	-3.8559	-3.8531
# SPLP iter.	314	308	305	316	308	319	315
# Newton iter.	687	904	741	756	749	782	902
CPU time (s)							
Total	2642.35	1876.04	1847.92	1562.44	1733.29	1520.73	968.43
$F(\boldsymbol{\rho})$	2287.84	1524.55	1503.31	1202.70	1464.60	1155.81	604.06
\mathbf{K}_T	217.67	242.79	222.47	233.43	174.84	185.27	134.99
RHS	33.77	40.12	42.44	54.76	43.21	56.22	7.62
Factorizations	2019.77	1221.37	1208.39	861.13	1215.83	859.42	367.86
Linear systems	16.63	20.27	30.01	53.38	30.72	54.90	93.59
$\nabla F(\boldsymbol{\rho})$	107.38	107.79	105.02	111.89	107.22	113.11	113.77
SPLP solving	151.46	148.18	146.67	150.21	146.36	152.98	152.73
Filtering	89.69	89.19	86.79	90.96	8.86	92.02	91.03
Other	5.98	6.33	6.13	6.68	6.25	6.81	6.84

attained with a fixed budget. For the gripper, there was almost no difference between the results, and for the slender beam the performance of the first five strategies was degraded when full convergence was required, mainly due to an increase on the number of iterations of Newton’s method, as mentioned above. The figure also reveals the relevance of applying the ICA scheme to the computation of the objective function gradient. In general, the strategies whose name end with **g** (i.e., those that use ICA for solving (15)) attained the best results, notably **upK03K100g**, that showed a consistent improvement when the stopping criterion was changed.

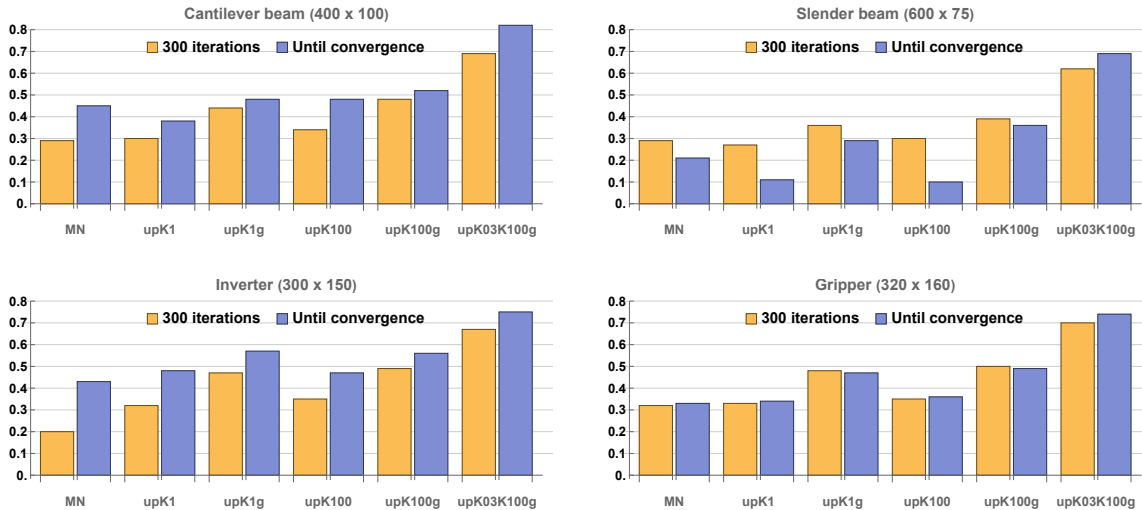


Figure 13: Percentage of decrease in the time required to evaluate the objective function, as compared to Newton’s method.

8 Investigating the behavior of the norm of matrix B

Let B be the matrix defined in (7). In Section 3, we demonstrated that if $\|B\| < 1$, then the sequence $\{s^{(k)}\}_{k=0}^{+\infty}$ (defined in (8) and associated with the ICA method) converges to the solution s^* of the linear system (4) of Newton’s method. Moreover, we showed that this sequence has linear rate of convergence.

With the aim of investigating the impact of the variation on the maximum value of $\|B\|_2$ attained whenever the nonlinear system (2) is solved, we have performed an additional test considering the slender beam and the gripper mechanism, using strategies **upK100g** and **upK03K100g**. Since the explicit evaluation of B is very expensive, these numerical test was performed in MATLAB (version R2016a) and took into account a coarser mesh, with $160 \times 20 = 3200$ finite elements for the slender beam and $80 \times 40 = 3200$ finite elements for the gripper mechanism, applying the stopping criterion for the SPLP method stated in (16).

As in the previous experiments, the optimal values of the objective function found in this new test were very similar for the two structures considered here, regardless of the applied strategy. For each combination of problem and strategy, we have recorded $\|B\|_2$ and the number of iterations of Newton’s method, to see how they vary along time. The results are shown in Figures 14 and 15.

We can observe that there is a direct relation between the number of iterations of Newton’s method and the value of $\|B\|_2$, i.e., the chance of performing more than 3 iterations increases with the norm of B . Even though, when the **upK100g** strategy is applied, the number of iterations necessary to find the approximate solution of the linear system (4) is at most equals to 3 in 93.5% of the iterations for the slender beam and 98.2% for the gripper. For the **upK03K100g** strategy, no more than 3 linear system solutions are required in 48.6% of the iterations for the slender

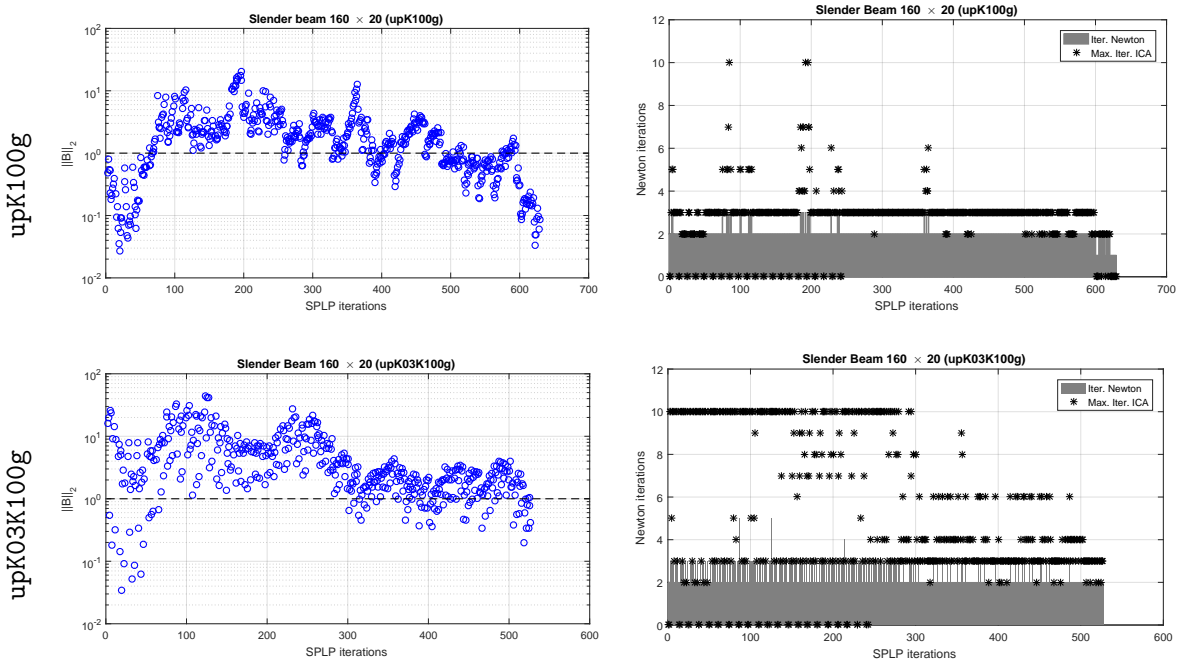


Figure 14: Maximum value of $\|B\|_2$ (left) and number of iterations of Newton's method (right) for the slender beam 160×20 .

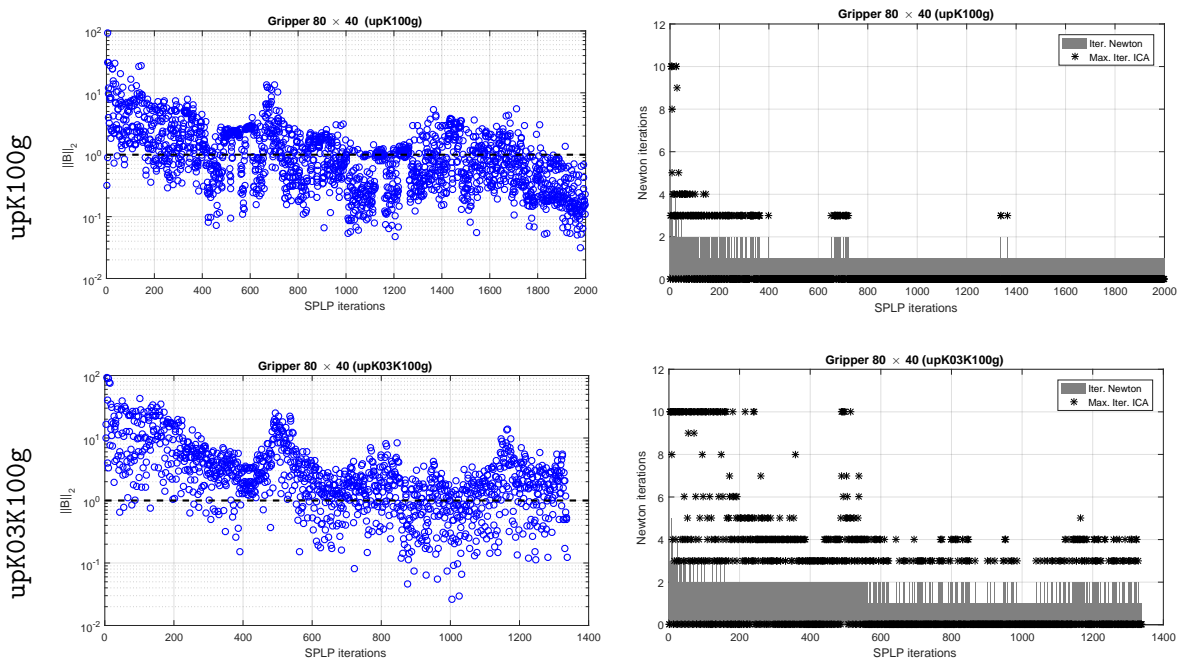


Figure 15: Maximum value of $\|B\|_2$ (left) and number of iterations of Newton's method (right) for the gripper 80×40 .

beam and 73.5% for the gripper.

As shown in Figures 14 and 15, when the `upK100g` strategy is used, the maximum value of $\|\mathbf{B}\|_2$ is below 1 in 41.7% of the SPLP iterations for the slender beam, and in 56.3% for the gripper. For the `upK03K100g` strategy, this percentage is reduced to 20.3% for the slender beam and 26.5% for the gripper. However, for both strategies, the approximate solution of the nonlinear system (2) was always obtained after at most 4 iterations of Newton’s method, no matter the problem under analysis. Therefore, we conclude that our reanalysis strategies are robust.

9 Final remarks

Under the geometric nonlinearity assumption, the nonlinear equations that model the equilibrium of topology optimization problems must be solved repeatedly along the solution process, constituting the bottleneck of any iterative scheme.

In this work, to accommodate the trade-off between speed and accuracy, five strategies have been proposed to steer the frequencies of the factorizations and of the updates along the solution process. These strategies have provided significant time savings as compared with Newton’s method, without spoiling the convergence behavior of the algorithm. Indeed, strategy `upK03K100g` has saved more than 60% with the fixed budget of 300 SPLP iterations, and around 70% when the solver is run up to convergence. The deformed structures and mechanisms obtained by means of this strategy are given in Appendix B.

By choosing four different finite element meshes, we have observed that the CPU time spent for evaluating the objective function scales well with the dimensions of the global stiffness matrix. Moreover, strategy `upK03K100g` produced the smallest rate of increase in time as the meshes were refined.

Despite the theoretical condition for convergence of the reanalysis, namely $\|\mathbf{B}\|_2 < 1$, not being verified all along the iterations, we have observed that the incidental increasing of such a norm did not have a negative impact upon the results, corroborating the robustness of the proposed strategies.

We have also observed that the use of the ICA scheme for solving the adjoint linear system associated with the sensitivity analysis had a crucial role in accelerating the SPLP algorithm. The combination of this scheme with the factorization of \mathbf{K}_T at every 3 iterations and the update of $\Delta\mathbf{K}$ at every 100 iterations of Newton’s method turned `upK03K100g` into a fast, yet robust, approach, outperforming the remaining strategies.

Related topics for future research include the mixing of the proposed strategies with further acceleration schemes, such as reduced-order modeling and multigrid methods, as well as handling additional stress constraints into the model (see e.g.[2, 13, 18]). Another room for investigation would be to admit geometric nonlinearities within the minimum weight problem formulation (cf. [1, 24]), to develop the inherent approximate reanalysis framework by means of iterative combined approximations, and to assess its impact.

Acknowledgements. This work was partially supported by *Fundação de Amparo à Pesquisa do Estado de São Paulo* (grants 2013/07375-0, 2018/24293-0); and *Conselho Nacional de Desenvolvimento Científico e Tecnológico* (grant 305010/2020-4).

References

- [1] O. Amir. Revisiting approximate reanalysis in topology optimization: on the advantages of recycled preconditioning in a minimum weight procedure. *Structural and Multidisciplinary Optimization*, 51:41–57, 2015.

- [2] O. Amir. Efficient stress-constrained topology optimization using inexact design sensitivities. *International Journal for Numerical Methods in Engineering*, 122:3241–3272, 2021.
- [3] O. Amir, U. Kirsch, and I. Sheinman. Efficient non-linear reanalysis of skeletal structures using combined approximations. *International Journal for Numerical Methods in Engineering*, 73:1328–1346, 2008.
- [4] O. Amir, O. Sigmund, B. S. Lazarov, and M. Schevenels. Efficient reanalysis techniques for robust topology optimization. *Computer Methods in Applied Mechanics and Engineering*, 245-246:217–231, 2012.
- [5] O. Amir, M. Stolpe, and O. Sigmund. Efficient use of iterative solvers in nested topology optimization. *Structural and Multidisciplinary Optimization*, 42:55–72, 2010.
- [6] M. P. Bendsoe. Optimal shape design as a material distribution problem. *Structural and Multidisciplinary Optimization*, 1:193–202, 1989.
- [7] M. P. Bendsoe and O. Sigmund. *Topology Optimization*. Springer-Verlag, Berlin Heidelberg, 2nd edition, 2004.
- [8] M. Bogomolny. Topology optimization for free vibrations using combined approximations. *International Journal for Numerical Methods in Engineering*, 82:617–636, 2010.
- [9] T. E. Bruns and D. A. Tortorelli. An element removal and reintroduction strategy for the topology optimization of structures and compliant mechanisms. *International Journal for Numerical Methods in Engineering*, 57:1413–1430, 2003.
- [10] Q. Chen, X. Zhang, and B. Zhu. A 213-line topology optimization code for geometrically nonlinear structures. *Structural and Multidisciplinary Optimization*, 59:1863–1879, 2019.
- [11] S. H. Chen and Z. J. Yang. A universal method for structural static reanalysis of topological modifications. *International Journal for Numerical Methods in Engineering*, 61:673–686, 2004.
- [12] Z. Cheng and H. Wang. A meshless-based local reanalysis method for structural analysis. *Computers and Structures*, 192:126–143, 2017.
- [13] H. Deng, P. S. Vulimiri, and A. C. To. An efficient 146-line 3d sensitivity analysis code of stress-based topology optimization written in MATLAB. *Optimization and Engineering*, 2021.
- [14] A. R. Díaz and O. Sigmund. Checkerboard patterns in layout optimization. *Structural and Multidisciplinary Optimization*, 10:40–45, 1995.
- [15] G. H. Golub and C. F. V. Loan. *Matrix Computations*. The Johns Hopkins University Press, Baltimore, Maryland, 4th edition, 2013.
- [16] F. A. M. Gomes and T. A. Senne. An algorithm for the topology optimization of geometrically nonlinear structures. *International Journal for Numerical Methods in Engineering*, 99:391–409, 2014.
- [17] Y. Han, B. Xu, and Y. Liu. An efficient 137-line matlab code for geometrically nonlinear topology optimization using bi-directional evolutionary structural optimization method. *Structural and Multidisciplinary Optimization*, 63:2571–2588, 2021.
- [18] E. Holmberg, B. Torstenfelt, and A. Klarbring. Stress constrained topology optimization. *Structural and Multidisciplinary Optimization*, 48:33–47, 2013.

- [19] L. Juanjuan and W. Hu. Fast sensitivity reanalysis methods assisted by independent coefficients and indirect factorization updating strategies. *Advances in Engineering Software*, 119:93–102, 2018.
- [20] U. Kirsch. *Reanalysis of Structures*. Springer, Dordrecht, 2008.
- [21] U. Kirsch. Reanalysis and sensitivity reanalysis by combined approximations. *Structural and Multidisciplinary Optimization*, 40:1–15, 2010.
- [22] R. D. Lahuerta, E. T. Simões, E. M. B. Campello, P. M. Pimenta, and E. C. N. Silva. Towards the stabilization of the low density elements in topology optimization with large deformation. *Computational Mechanics*, 52:779–797, 2013.
- [23] H. Liu, B. Wu, and Z. Li. Preconditioned conjugate gradient method for static reanalysis with modifications of supports. *Journal of Engineering Mechanics*, 141:04014111, 2014.
- [24] K. Long, C. Gu, X. Wang, J. Liu, Y. Du, Z. Chen, and N. Saeed. A novel minimum weight formulation of topology optimization implemented with reanalysis approach. *International Journal for Numerical Methods in Engineering*, 120:567–579, 2019.
- [25] S. Mukherjee, D. Lu, B. Raghavan, P. Breitkopf, S. Dutta, M. Xiao, and W. Zhang. Accelerating large-scale topology optimization: State-of-the-art and challenges. *Archives of Computational Methods in Engineering*, Online first, 2021.
- [26] M. N. Nguyen, N. T. Nguyen, T. T. Truong, and T. Q. Bui. An efficient reduced basis approach using enhanced meshfree and combined approximation for large deformation. *Engineering Analysis with Boundary Elements*, 133:319–329, 2021.
- [27] J. Nocedal and S. J. Wright. *Numerical Optimization*. Springer, New York, NY, USA, 2nd edition, 2006.
- [28] T. A. Senne, F. A. M. Gomes, and S. A. Santos. On the approximate reanalysis technique in topology optimization. *Optimization and Engineering*, 20:251–275, 2019.
- [29] B. Zhu, X. Zhang, H. Li, J. Liang, R. Wang, H. Li, and S. Nishiwaki. An 89-line code for geometrically nonlinear topology optimization written in freefem. *Structural and Multidisciplinary Optimization*, 63:1015–1027, 2021.
- [30] W. Zuo, J. Bai, and J. Yu. Sensitivity reanalysis of static displacement using Taylor series expansion and combined approximate method. *Structural Multidisciplinary Optimization*, 53:953–959, 2016.
- [31] W. Zuo, Z. Yu, S. Zhao, and W. Zhang. A hybrid Fox and Kirsch’s reduced basis method for structural static reanalysis. *Structural Multidisciplinary Optimization*, 46:262–272, 2012.

A Results obtained for 300 iterations of SPLP

Table 5: Results obtained for 300 iterations of SPLP (Slender beam 200×25).

Slender beam 200 × 25	N	MN	upK1	upK1g	upK100	upK100g	upK03 K100g
$F(\boldsymbol{\rho})$ - value	134.81	134.81	134.81	134.81	134.81	134.81	134.81
# Newton iter.	712	1420	792	792	793	793	887
CPU time (s)							
Total	77.68	82.50	69.11	66.86	62.97	59.27	48.25
$F(\boldsymbol{\rho})$	66.93	70.72	58.24	55.85	52.04	48.25	36.26
\mathbf{K}_T	22.49	36.02	25.20	26.81	18.71	19.59	13.14
RHS	3.04	5.39	4.32	5.14	4.35	5.18	6.91
Factorizations	40.36	27.38	25.88	19.79	26.06	19.34	10.61
Linear systems	1.04	1.93	2.84	4.11	2.92	4.14	5.60
$\nabla F(\boldsymbol{\rho})$	1.15	1.25	1.17	1.23	1.14	1.28	1.31
SPLP solving	9.40	10.32	9.49	9.57	9.59	9.53	10.08
Filtering	0.16	0.17	0.17	0.17	0.16	0.17	0.20
Other	0.04	0.04	0.04	0.04	0.04	0.04	0.40

Table 6: Results obtained for 300 iterations of SPLP (Slender Beam 400×50).

Slender beam 400 × 50	N	MN	upK1	upK1g	upK100	upK100g	upK03 K100g
$F(\boldsymbol{\rho})$ - value	136.88	136.88	136.88	136.88	136.88	136.88	136.88
# Newton iter.	659	975	727	727	727	727	872
CPU time (s)							
Total	463.66	395.47	379.82	348.30	364.02	324.34	292.08
$F(\boldsymbol{\rho})$	366.68	298.04	282.30	248.50	265.01	226.43	187.72
\mathbf{K}_T	86.36	103.34	89.72	92.11	70.75	71.93	53.17
RHS	12.35	16.10	14.07	17.09	14.27	16.70	29.80
Factorization	262.93	171.85	170.85	127.55	172.28	125.99	74.67
Linear system	5.04	6.75	7.66	11.75	7.71	11.81	30.08
$\nabla F(\boldsymbol{\rho})$	10.63	10.70	10.59	10.75	10.61	10.82	11.40
SPLP solving	79.78	80.15	80.33	82.34	81.70	80.51	85.89
Filtering	6.07	6.08	6.10	6.21	6.20	6.08	6.54
Other	0.50	0.50	0.50	0.50	0.50	0.50	0.53

Table 7: Results obtained for 300 iterations of SPLP (Slender beam 600×75).

Slender beam 600 × 75	N	MN	upK1	upK1g	upK100	upK100g	upK03 K100g
$F(\boldsymbol{\rho})$ - value	138.62	138.52	138.68	138.77	138.68	138.77	138.62
# Newton iter.	648	758	658	667	658	670	838
CPU time (s)							
Total	1622.93	1262.76	1293.72	1201.68	1263.94	1170.56	876.84
$F(\boldsymbol{\rho})$	1208.74	853.88	878.07	770.80	846.39	741.24	463.44
\mathbf{K}_T	189.38	210.10	191.42	199.88	157.05	162.87	106.44
RHS	26.97	30.74	29.07	43.71	29.01	46.34	59.35
Factorization	979.93	599.03	640.57	480.06	643.33	479.84	232.96
Linear system	12.46	14.01	17.01	47.15	17.00	52.19	64.69
$\nabla F(\boldsymbol{\rho})$	34.74	35.33	35.09	35.12	35.06	35.37	35.35
SPLP solving	351.85	345.64	352.93	367.64	354.74	365.88	350.45
Filtering	25.71	25.97	25.73	26.23	25.86	26.16	25.69
Other	1.89	1.94	1.90	1.89	1.89	1.91	1.91

Table 8: Results obtained for 300 iterations of SPLP (Slender beam 800×100).

Slender beam 800 × 100	N	MN	upK1	upK1g	upK100	upK100g	upK03 K100g
$F(\boldsymbol{\rho})$ - value	140.22	140.22	140.04	140.23	140.04	140.04	140.04
# Newton iter.	649	754	650	656	650	582	830
CPU time (s)							
Total	4068.97	3365.41	3275.92	3014.94	3233.85	2830.65	2485.81
$F(\boldsymbol{\rho})$	2454.18	1746.14	1660.74	1390.40	1610.00	1277.13	861.18
\mathbf{K}_T	336.94	336.89	349.12	360.41	280.64	254.73	185.56
RHS	48.22	53.72	52.21	77.82	51.67	52.11	102.37
Factorizations	2045.59	1329.63	1238.12	865.55	1246.52	932.81	462.46
Linear systems	23.43	25.90	21.29	86.62	31.17	37.48	109.79
$\nabla F(\boldsymbol{\rho})$	261.85	267.79	266.58	269.33	266.78	242.10	274.78
SPLP solving	1107.07	1106.43	1102.45	1109.93	1112.00	1085.03	1103.35
Filtering	229.20	228.41	229.45	228.28	228.40	206.20	229.25
Other	16.67	16.64	16.70	17.00	16.67	20.19	17.25

Table 9: Results obtained for 300 iterations of SPLP (Inverter 200×100).

Inverter 200 × 100	N	MN	upK1	upK1g	upK100	upK100g	upK03 K100g
$F(\boldsymbol{\rho})$ - value	-6.9372	-6.9374	-6.9375	-6.9330	-6.9330	-6.9373	-6.9371
# Newton iter.	680	928	850	833	833	853	923
CPU time (s)							
Total	589.85	427.84	432.10	362.21	412.60	342.83	257.88
$F(\boldsymbol{\rho})$	536.27	373.98	377.97	307.35	358.16	287.61	202.73
\mathbf{K}_T	72.27	82.49	79.33	80.00	56.82	59.24	48.24
RHS	12.26	15.45	17.98	22.45	17.78	23.07	29.35
Factorizations	446.15	268.96	269.07	184.50	272.20	184.17	93.75
Linear systems	5.59	7.08	11.59	20.40	11.36	21.13	31.39
$\nabla F(\boldsymbol{\rho})$	10.68	10.79	10.80	11.08	10.79	11.06	11.07
SPLP solving	36.29	36.40	36.67	37.02	37.02	37.47	37.38
Filtering	6.15	6.20	6.19	6.29	6.16	6.22	6.23
Other	0.46	0.47	0.47	0.47	0.47	0.47	0.47

Table 10: Results obtained for 300 iterations of SPLP (Inverter 300×150).

Inverter 300 × 150	N	MN	upK1	upK1g	upK100	upK100g	upK03 K100g
$F(\boldsymbol{\rho})$ - value	-8.6969	-8.6989	-8.7020	-8.7035	-8.6997	-8.7028	-8.7046
# Newton iter.	696	1065	859	849	848	841	929
CPU time (s)							
Total	1883.89	1334.16	1344.36	1097.37	1293.52	1066.04	756.60
$F(\boldsymbol{\rho})$.	1691.98	1144.86	1149.91	905.20	1102.38	860.02	564.05
\mathbf{K}_T	161.20	194.80	178.60	179.35	128.35	132.06	106.75
RHS	28.87	38.90	42.83	54.16	42.22	54.37	66.69
Factorizations	1487.78	891.76	895.51	614.71	899.80	616.35	310.82
Linear systems	14.13	19.40	32.97	56.98	31.98	57.24	79.79
$\nabla F(\boldsymbol{\rho})$	35.44	36.17	37.69	36.37	36.27	36.61	36.57
SPLP solving	128.50	124.56	126.68	126.87	126.22	140.25	127.22
Filtering	26.23	26.77	28.17	27.09	26.88	27.29	26.90
Other	1.74	1.80	1.91	1.84	1.77	1.87	1.86

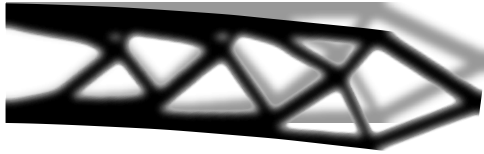
Table 11: Results obtained for 300 iterations of SPLP (Inverter 400×200).

Inverter 400 × 200	N	MN	upK1	upK1g	upK100	upK100g	upK03 K100g
$F(\boldsymbol{\rho})$ - value	-8.4352	-8.4342	-8.4356	-8.4352	-8.4355	-8.4399	-8.4362
# Newton iter.	700	930	797	783	784	804	903
CPU time (s)							
Total	4827.72	3482.96	3501.80	2845.28	3408.99	2823.02	2123.78
$F(\boldsymbol{\rho})$	3924.52	2575.07	2580.67	1959.74	2502.04	1893.70	1191.78
\mathbf{K}_T	286.57	324.00	302.85	308.58	227.14	236.92	190.77
RHS	51.31	62.80	68.74	86.44	67.57	87.90	111.88
Factorization	3559.94	2155.70	2158.38	1476.52	2157.75	1478.63	753.57
Linear system	26.70	32.57	50.70	88.20	49.58	90.25	135.56
$\nabla F(\boldsymbol{\rho})$	268.66	273.07	272.17	264.29	273.24	283.94	286.48
SPLP solving	385.21	383.65	398.97	378.80	383.87	388.66	390.09
Filtering	233.72	235.29	234.31	226.75	234.06	239.92	238.60
Other	15.61	15.88	15.68	15.70	15.78	17.40	16.83

Table 12: Results obtained for 300 iterations of SPLP (Inverter 500×250).

Inverter 500 × 250	N	MN	upK1	upK1g	upK100	upK100g	upK03 K100g
$F(\boldsymbol{\rho})$ - value	-7.7597	-7.7599	-7.7600	-7.7598	-7.7597	-7.7595	-7.7596
# Newton iter.	673	823	741	745	750	747	864
CPU time (s)							
Total	10214.38	7165.38	7186.63	5867.43	7060.42	5703.46	4334.30
$F(\boldsymbol{\rho})$	8306.03	5285.67	5295.14	3944.25	5157.13	3818.24	2394.37
\mathbf{K}_T	549.73	594.25	570.72	582.55	440.70	450.47	298.57
RHS	90.72	91.38	101.18	128.63	102.14	127.72	169.83
Factorizations	7618.48	4547.31	4549.31	3102.94	4538.28	3111.46	1694.96
Linear systems	47.10	52.73	73.72	130.13	76.01	128.59	231.01
$\nabla F(\boldsymbol{\rho})$	669.89	662.19	671.27	690.44	672.98	659.28	717.43
SPLP solving	597.88	577.06	576.98	588.24	584.80	579.47	578.53
Filtering	601.68	601.35	604.05	603.05	605.36	604.38	599.50
Other	38.90	39.11	39.09	41.45	39.15	42.09	44.47

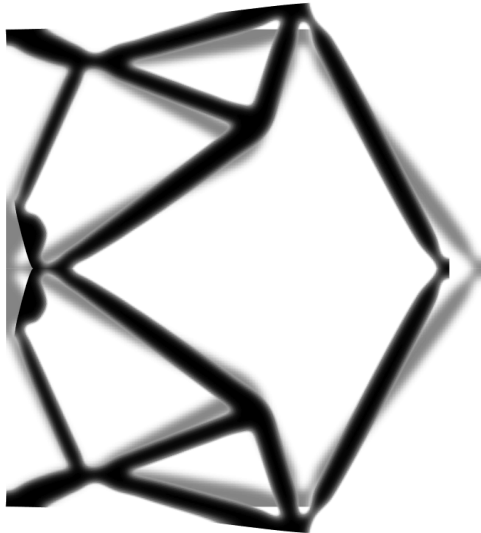
B Final configurations



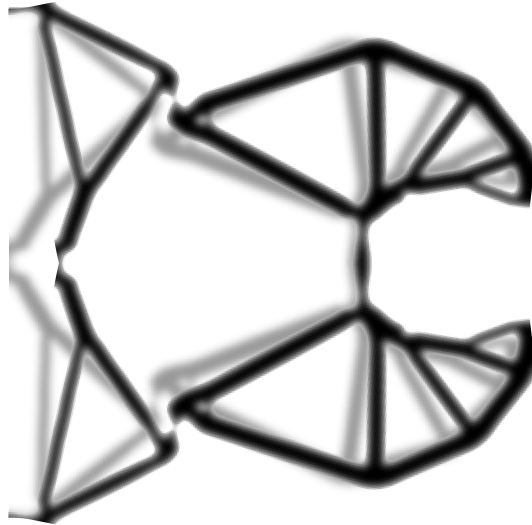
cantilever beam (400×100)



slender beam (800×100)



inverter (500×250)



gripper (320×160)

Figure 16: Final configurations of the instances with large displacements (reached by the upK03K100g strategy). The darker structures and mechanisms highlight the attained deformations with respect to the lighter gray ones.